The Helmholtz-Hodge Decomposition—A Survey

Harsh Bhatia, *Student Member, IEEE*, Gregory Norgard,
Valerio Pascucci, *Member, IEEE*, and Peer-Timo Bremer, *Member, IEEE*

Abstract—The *Helmholtz-Hodge Decomposition (HHD)* describes the decomposition of a flow field into its divergence-free and curl-free components. Many researchers in various communities like weather modeling, oceanology, geophysics, and computer graphics are interested in understanding the properties of flow representing physical phenomena such as incompressibility and vorticity. The HHD has proven to be an important tool in the analysis of fluids, making it one of the fundamental theorems in fluid dynamics. The recent advances in the area of flow analysis have led to the application of the HHD in a number of research communities such as flow visualization, topological analysis, imaging, and robotics. However, because the initial body of work, primarily in the physics communities, research on the topic has become fragmented with different communities working largely in isolation often repeating and sometimes contradicting each others results. Additionally, different nomenclature has evolved which further obscures the fundamental connections between fields making the transfer of knowledge difficult. This survey attempts to address these problems by collecting a comprehensive list of relevant references and examining them using a common terminology. A particular focus is the discussion of boundary conditions when computing the HHD. The goal is to promote further research in the field by creating a common repository of techniques to compute the HHD as well as a large collection of example applications in a broad range of areas.

Index Terms—Vector fields, incompressibility, boundary conditions, Helmholtz-Hodge decomposition

◆

1 INTRODUCTION

THE *Helmholtz-Hodge Decomposition (HHD)* of vector fields is one of the fundamental theorems in fluid dynamics. It describes a vector field in terms of its divergence-free and rotation-free components. Such a description simplifies the analysis of vector fields since some important properties like incompressibility and vorticity can be studied on the components directly.

Due to the ubiquitous nature of vector fields, this fundamental theorem of fluid motion has been applied by various research communities to a wide variety of applications. More theoretically inclined communities like fluid mechanics, physics, and mathematics have developed projection methods [19], [20] which employ the decomposition for the simulation of incompressible fluids using the Navier-Stokes equation (NSE). Since many simulated domains have boundaries, different boundary conditions and their impact on the decomposition have received special attention. Other communities have focused primarily on exploiting the different properties of the HHD to, for example, create more realistic visualizations of fluids [34],

[92], detect singularities [83], [84], or to smooth vector fields [97]. Application areas span everything from visualization and computer graphics, to astrophysics [40], [67], [95], geophysics [3], [4], computer vision and robotics [38], [43], [44], [73], imaging [52], etc. In all these applications, the HHD plays a key role in modeling, analyzing, or manipulating fluids.

1.1 Motivation

As discussed above, a variety of research communities are actively exploring techniques to compute and apply the HHD. Nevertheless, while there exist cases of successful knowledge transfer (see, for example, the vision and robotics research in Fig. 1) most advances are made within a given community. Furthermore, through multiple derivations seemingly minor details such as boundary conditions can get lost resulting in a sometimes confusing and contradictory publication record.

For example, Stam [92] follows the HHD as defined by Chorin and Marsden [22] and adapts it for a specific no-flow boundary setting. Under such a setting, a Neumann boundary condition can be imposed on the decomposition, while Colin et al. [23] discuss the same Neumann boundary conditions without a no-flow setting, in which orthogonality, a very important and much desired property of the decomposition is lost. Subsequently, following both Colin and Stam, Petronetto et al. [81] comment that the usual boundary conditions in the general case are Neumann boundary conditions. Thus, while every publication inspires new research, older results can be overlooked in a multilayered literature.

One particular detail of interest are the boundary conditions and their influence on the results of the decomposition. In his diploma thesis, Wiebel [101] following Polthier and

- *H. Bhatia and P.-T. Bremer are with the Scientific Computing and Imaging Institute (SCI), University of Utah, and Center of Applied Scientific Computing, Lawrence Livermore National Laboratory, Box 808, L-422, Livermore, CA 94551-0808. E-mail: {hbhatia, ptbremer}@sci.utah.edu.*
- *G. Norgard is with Numerica, 3330 Red Mountain Dr., Fort Collins, CO 80525. E-mail: gregnorgard@gmail.com.*
- *V. Pascucci is with the Scientific Computing and Imaging Institute (SCI), University of Utah, 72 S Central Campus Drive, Room 3750, Salt Lake City, UT 84112. E-mail: pascucci@sci.utah.edu.*
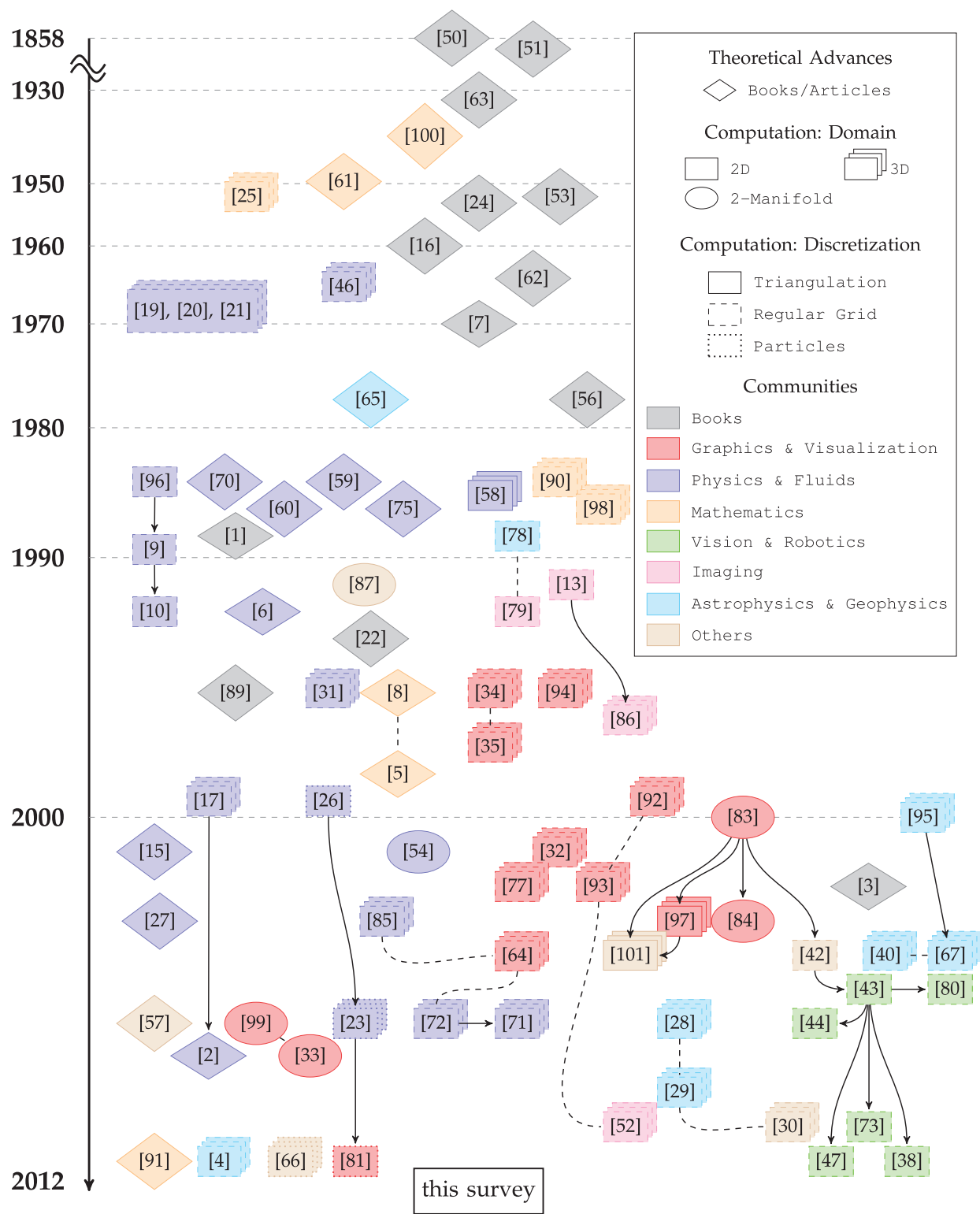
Fig. 1. A chronological chart showing the articles on HHD. The different shapes classify the articles into theoretical advances and computation techniques for different domains and discretizations. Different colors classify the articles into the communities they were published in (as tabulated in Table 1). Solid arrows and dashed lines between two articles represent a direct inheritance or extension, and a weaker connection between them, respectively.

Preuß [83], [84], and Tong et al. [97] comments that there exist failure cases of the 2D HHD. More specifically, he shows that if critical points lie on or near the boundary of the domain, the structure of the decomposed components of the field is changed significantly. We argue that such artifacts should be attributed to the boundary conditions of the decomposition, which are needed to maintain orthogonality. Orthogonality is a delicate issue in HHD and has been studied thoroughly in literature. However, in the recent approaches, especially in the visualization community, there has been little discussion

TABLE 1
Classification of Various Journals, Conferences and Workshops into Communities Shown in Fig. 1

Community	Journal [J], Conference [C], Workshop [W] ?
Graphics & Visualization	[J] ACM Computer Graphics (Annual Conference Series); ACM Transactions on Graphics; Graphical Models and Image Processing; IEEE Transactions on Visualizations and Computer Graphics; Journal of Graphics Tools; Mathematical Visualization III [C] ACM SIGGRAPH [W] Eurographics Workshop on Scientific Visualization
Physics & Fluids	[J] American Journal of Physics; Annual Review of Fluid Mechanics; Computational Mechanics; International Journal for Numerical Methods in Physics; Journal of Computational Physics; Mathematics of Computation; Physics of Fluids; SIAM Journal on Numerical Analysis
Mathematics	[J] Annals of Mathematics; Communication on Pure and Applied Mathematics; Duke Mathematical Journal; Mathematical Methods in the Applied Sciences; Nonlinear Methods in Applied Mathematics; SIAM Journal on Scientific and Statistical Computing [C] International Symposium on Computer Methods for Partial Differential Equations
Vision & Robotics	[J] Computers in Biology and Medicine; LNCS Pattern Recogntion and Machine Intelligence; Pattern Recognition Letters [C] IEEE International Conference on Acoustics Speech and Signal Processing; IEEE International Conference on Robotics and Automation; International Conference on Image and Vision Computing
Imaging	[J] IEEE Transactions on Image Processing; IEEE Transactions on Signal Processing [C] International Conference on Information Processing in Medical Imaging
Astrophysics & Geophysics	[J] The Astronomical Journal; Geophysics Journal International; International Journal on Geomathematics; Journal of Turbulence; NASA Center for Turbulence Research - Annual Research Briefs; Solar Physics; SIAM Multiscale Modeling and Simulation [W] SOHO14/GONG 2004 Workshop
Others	[J] Proceedings of the National Academy of Sciences (PNAS) [C] Southeastern Symposium on System Theory Technical Reports, PhD/Master's Theses

on orthogonality of the decomposition, and hence, a more thorough understanding of the interplay between orthogonality and boundary conditions is needed.

While there already exist some excellent review papers on related topics, their scope is typically limited. For example, Aref et al. [6] and Morino [75] review the Helmholtz decomposition in context of vorticity problems, Joseph [57] discusses it in context of viscous fluids, Kobe [60] reviews the connection between Helmholtz and Hodge decompositions, and Srössig [91] describes generalizations of the Helmholtz decomposition for different domains. Nevertheless, there is a need for a more detailed study of the HHD that discusses the relevant theory from a broader perspective and in particular includes techniques to compute the discrete HHD. We believe that this comprehensive survey will aid future studies and help avoid diverging research branches by creating a common repository of references and techniques described in a single consistent terminology.

1.2 Contributions

This survey aims to explain the theory behind the HHD in a notationally consistent manner, discussing the effects of boundary conditions, and surveying the recent advances in computing the discrete HHD. We introduce the fundamentals of the decomposition from a historic point of view and summarize the theory presented in different books and articles. We provide a thorough discussion on boundary conditions highlighting any existing discrepancies between different articles. Additionally, we survey the different techniques proposed in various communities regarding the computation of the HHD.

The remainder of this survey is structured as follows: Section 3 investigates the origin and history of the

decomposition. It establishes the mathematical foundations of the decomposition in a consistent notation and refers the reader to the appropriate literature for a more detailed discussion. Section 4 introduces several relevant applications using the HHD surveyed from various communities. Section 5 discusses the interconnection between orthogonality and boundary conditions, highlighting existing discrepancies in recent articles. Finally, Section 6 surveys the most common techniques to compute the discretized for of the HHD.

2 THE HISTORY OF THE HHD

We begin with studying Fig. 1, which provides a chronological chart summarizing the publication history of the HHD, classifying some important books and articles into: 1) theoretical advances and computation techniques for different domains and discretizations, and 2) different research communities. This visual summary highlights the different research trends, as well as the connections between various communities. Since its introduction in 1858, the subject of HHD has been studied in various communities. Under the umbrella of projection methods, the computational fluids community has consistently used and refined them because their first development in the 1960s.

With its development in 1990s, the graphics and visualization community started making use of the projection methods in fluid modeling and animation. While virtually every article in fluid animation uses projection methods, only a few important articles dealing especially with computing the HHD are shown. The seminal paper by Polthier and Preuß [83] in 2000 proposes a new technique for the computation of discrete HHD, which has led to a renewed interest in the topic. Their ideas are introduced to

the computer vision and robotics community by Guo et al. [42], who further propose extensions tailored to the particular application. Similarly, Stam's ideas [92], [93] have inspired Hinkle et al. [52] to use the HHD in the Fourier domain for applications in imaging. Recent advantages in the visualization community by Petronetto et al. [81] draw their inspiration from Colin et al. [23] in computational physics community. Overall, Fig. 1 summarizes the different research thrusts and the connections between them, some of which will be discussed in more detail in this survey.

3 THEORY

This section investigates the theoretical foundations of the HHD and describes its mathematical properties in general. We begin with discussing the origin and theory of the Helmholtz decomposition of vector fields. While the Helmholtz decomposition is defined for vector fields on real domains, another decomposition, called the Hodge decomposition, exists, which is defined for differentiable forms on Riemannian manifolds. For completeness, we discuss the Hodge decomposition in Section 3.2. This brief discussion assumes some basic knowledge of the Hodge-de Rham theory, and can be skipped by readers only interested in understanding the fundamentals of the vector field (Helmholtz) decomposition. Then, we present the HHD as used in modern day research, which defines the decomposition of vector fields on domains with or without boundary.

Before we begin, it is worth mentioning that different applications and researchers have used different names (any of the following: Helmholtz, Hodge, Helmholtz-Hodge, or Hodge-Helmholtz) for the decomposition. As shown in Section 3.3, the decomposition may define two or three nonzero components. However, since in the case of vector fields, this difference is only due to the domain and boundary conditions, the motivation to choose one name over the other seems rather subjective, and conceptually, these names can be used interchangeably. Hence, we wish to warn the reader not to get confused when encountering different names. Irrespective of the name used, the theory behind the underlying decomposition should be clearly understood.

3.1 The Helmholtz Decomposition Theorem

In 1858, Prof. Hermann von Helmholtz, in his seminal paper, *Über Integrale der hydrodynamischen Gleichungen, welche den Wirbelbewegungen entsprechen* [50] explained how potential functions can be used to extract the rotational and irrotational components from a flow field. Following its success and popularity, an english translation *On Integrals of the Hydrodynamical Equations, which express Vortex-motion* was published in The Philosophical Magazine by P. G. Tait [51].

In [50, Section 1], Helmholtz explained that the motion of a volume element of a continuous fluid media in $\mathbb{R}^3$ consists of: 1) expansion or contraction in three orthogonal directions, 2) rotation about an instantaneous axis, and 3) translation. The expansion/contraction can be represented as the gradient of a scalar potential function because

it is irrotational. Similarly, the rotation can be represented as the curl of a vector potential function since it is incompressible. Translation, however, being both incompressible and irrotational can be represented as either the gradient of a scalar potential, or the curl of a vector potential. Equivalently, the translation can also be represented as a separate harmonic component. We will come back to the discussion on the harmonic component. For now, we discuss Helmholtz's original ideas, which represent the translation as the gradient of a scalar potential (with the irrotational component).

According to Helmholtz, under suitable asymptotic behavior at infinity, any vector field in $\mathbb{R}^3$ consists of two parts:

1. The first part is incompressible representing the rotation, and can be expressed as the curl of a vector potential function.
2. The second part is irrotational representing translation and compression/expansion, and can be expressed as the gradient of a scalar potential function.

These scalar and vector potentials can be computed from the divergence and the curl of the vector field. Thus, when its divergence and the curl are known, a vector field can be uniquely constructed. An excellent summary of Helmholtz's ideas is given by Lamb [63], who formulates them as follows:

Theorem 3.1 (Helmholtz Decomposition). *The motion of a fluid $\vec{\xi}(x)$ in an infinite space ($x \in \mathbb{R}^3$) such that it vanishes at infinity is determinate when we know the values of $\theta(x)$ and $\vec{\omega}(x)$, where*

$$\begin{aligned} \theta(x) &= \nabla \cdot \vec{\xi}(x) \quad (Divergence) \\ \vec{\omega}(x) &= \nabla \times \vec{\xi}(x) \quad (Curl). \end{aligned} \tag{1}$$

On the other hand, if the motion of the fluid is limited to a simply connected region $\Omega \subset \mathbb{R}^3$ with boundary $\partial\Omega$, it is determinate if $\theta(x)$, $\vec{\omega}(x)$ and the value of the flow normal to the boundary, $\xi_n(x)$ ($= \vec{\xi}(x) \cdot \vec{n}$) for $x \in \partial\Omega$, are known.

In later theoretical advances, an inverse problem to Helmholtz's ideas was formalized, which decomposes a given vector field into its divergence-free (incompressible) and curl-free (irrotational) components. This inverse problem is also called the *Helmholtz Decomposition*. The inverse problem states that any smooth vector field $\vec{\xi} : \mathbb{R}^3 \to \mathbb{R}^3$ can be expressed as a sum of the gradient of a scalar potential and the curl of a vector potential:

$$\vec{\xi} = \nabla D + \nabla \times \vec{R}, \tag{2}$$

where the scalar potential D and the vector potential $\vec{R}$ are calculated from θ and $\vec{\omega}$, respectively, as:

$$\begin{aligned} D(x) &= -\frac{1}{4\pi} \int \frac{\theta(x')}{|x - x'|} dx' \\ \vec{R}(x) &= \frac{1}{4\pi} \int \frac{\vec{\omega}(x')}{|x - x'|} dx'. \end{aligned} \tag{3}$$

By definition, ∇D is curl-free ($\nabla \times \nabla D = 0$) and $\nabla \times \vec{R}$ is divergence-free ($\nabla \cdot \nabla \times \vec{R} = 0$).

In 1905, Blumenthal [12] proved the uniqueness of the decomposition. The vanishing condition at infinity is imposed to ensure that the integrals in (3) converge. Note that the potentials D and $\vec{R}$ are unique up to a constant; hence, the decomposition is unique. Similarly, for domains with boundaries, the normal velocity ξ_n is required to ensure uniqueness.[1]

Since its introduction, the Helmholtz decomposition theorem has been thoroughly discussed in general. It has also been investigated in different domains like smooth L_r spaces [36], convex domains [39] and antisymmetric second-rank tensor fields [59]. Hauser [48], [49] generalized Helmholtz's theorem to $\mathbb{R}^4$ by proving it for second-rank tensors. A recent article by Sprössig [91] gives a brief overview of the variants of the Helmholtz theorem under specific or general conditions and domains.

Note that under the vanishing condition at infinity, the translation (harmonic component) is zero. However, in the case of a bounded domain, a nonzero harmonic (irrotational and incompressible) component may be present. Such a decomposition is called the Hodge decomposition. For domains with boundary, the harmonic component is zero if the flow on the boundary is zero, and for simply connected domains, this harmonic component can be represented by either ∇D or $\nabla \times \vec{R}$. Hence, the normal velocity ξ_n is required to ensure that the translation is represented entirely by the irrotational component leading to a unique decomposition.[1]

3.2 The Hodge Decomposition Theorem

Similar to the Helmholtz decomposition for vector fields, a decomposition called the Hodge decomposition, named after W. V. D. Hodge, exists for differential forms. The theory of differential forms is intended to perform multivariable calculus with a more generalized viewpoint, i.e., independent of the coordinates. Using the calculus defined on the differential forms, it is possible to generalize the vector analysis from real domains ($\mathbb{R}^n$) to differentiable manifolds. The Hodge decomposition decomposes a differential k-form defined on a Riemannian manifold into three mutually L^2-orthogonal components.

We briefly discuss the theorem as described by Abraham et al. [1]. For details on Hodge de Rham theory, harmonic fields and Hodge decomposition the reader may refer to [53], [61], [89]. In the following theorem, $\Omega^k(\mathcal{M})$ is the space of smooth, weakly differentiable k-forms on the manifold $\mathcal{M}$, $\vec{d}$ is the exterior derivative on k-forms, $\vec{\delta}$ is the codifferential operator, and $\mathcal{H}$ denotes the vector space of harmonic k-forms, such that

$$\mathcal{H}^k(\mathcal{M}) = \{\alpha \in \Omega^k(\mathcal{M}) \mid \vec{d}\alpha = 0, \ \vec{\delta}\alpha = 0\}.$$

Theorem 3.2 (Hodge Decomposition). *Let $\mathcal{M}$ be a compact, boundaryless, oriented, Riemannian manifold. Then, the space of differential k-forms on $\mathcal{M}$, $\Omega(\mathcal{M})$ can be decomposed as a direct sum of the exterior derivative of a $k-1$ form, the codifferential of a $k+1$ form, and a harmonic k-form. The three components are mutually L^2-orthogonal, and thus are uniquely determined*

1. For proof of uniqueness, see Section 3.3.1.

$$\Omega^k = \vec{d}\Omega^{k-1} \ \oplus \ \vec{\delta}\Omega^{k+1} \ \oplus \ \mathcal{H}^k.$$

In other words, if $\omega \in \Omega^k(\mathcal{M})$, then ω can be decomposed as

$$\omega = \vec{d}\alpha + \vec{\delta}\beta + \gamma,$$

such that $\alpha \in \Omega^{k-1}(\mathcal{M}), \beta \in \Omega^{k+1}(\mathcal{M}), \gamma \in \mathcal{H}^k(\mathcal{M})$. Furthermore, $\vec{d}\alpha, \vec{\delta}\beta,$ and γ are mutually L^2-orthogonal, and thus are uniquely determined.

On the other hand, if $\mathcal{M}$ is a compact, oriented, Riemannian manifold with boundary $\partial\mathcal{M}$, then the decomposition takes the form

$$\Omega^k = \vec{d}\Omega_t^{k-1} \ \oplus \ \vec{\delta}\Omega_n^{k+1} \ \oplus \ \mathcal{H}^k,$$

where

$$\Omega_t^{k-1}(\mathcal{M}) = \{\alpha \in \Omega^{k-1}(\mathcal{M}) \mid \alpha \text{ is parallel to } \partial\mathcal{M}\}$$
$$\Omega_n^{k+1}(\mathcal{M}) = \{\alpha \in \Omega^{k+1}(\mathcal{M}) \mid \alpha \text{ is normal to } \partial\mathcal{M}\}.$$

Here, parallel and normal are defined with respect to the metric defined on the Riemannian manifold [1].

The Hodge decomposition is closely related to the Helmholtz decomposition, although, the former is not a direct generalization of the latter. A study of differential forms as a basis for vector analysis was provided by Schleifer [88], who commented that the Hodge decomposition is the differential form analog of the Helmholtz decomposition in vector analysis. Cantarella et al. [18] provide an insightful discussion on the topology of mutually orthogonal vector spaces in three dimensions, and Schwarz [89] provides an extensive discussion on the generalized Hodge decomposition for nonsimply connected domains.

3.3 The Helmholtz-Hodge Decomposition (HHD)

In this section, we will discuss the HHD of vector fields. While to the best of our knowledge, there is no known origin of the *Helmholtz-Hodge Decomposition Theorem*, or a formal merging of the names Helmholtz and Hodge, Denaro [27] attributes it to Ladyzhenksaya [62]. For the remainder of this paper, we restrict our attention to the simply connected domains with boundary.

3.3.1 HHD—Two Component Form

Most of the modern day research refers to the HHD as presented by Chorin and Marsden [22] which is:

Let $\vec{\xi}$ be a sufficiently smooth vector field on a bounded domain Ω, with a smooth boundary $\partial\Omega$. Then, $\vec{\xi}$ can be uniquely decomposed in the form

$$\vec{\xi} = \nabla D + \vec{r},$$

where D is a scalar potential function, the vector field $\vec{r}$ has zero divergence and is tangential to the boundary along $\partial\Omega$.

Chorin and Marsden [22] state the boundary condition $\vec{r} \cdot \vec{n} = 0$ for the decomposition, and prove the existence, orthogonality, and uniqueness of the decomposition under this condition. Denaro [27] proves the existence, orthogonality, and uniqueness for an additional boundary condition, which states that the irrotational component is normal to the boundary ($\vec{n} \times \vec{d} = 0$). His version of the HHD states that:

A vector field $\vec{\xi}$ is uniquely determined when its divergence $(\nabla \cdot \vec{\xi})$ and curl $(\nabla \times \vec{\xi})$ are assigned, along with the normal $(\xi_n = \vec{n} \cdot \vec{\xi})$ or tangential $(\vec{\xi}_t = \vec{n} \times \vec{\xi})$ component on the boundary

$$\vec{\xi} = \nabla D + \nabla \times \vec{R}$$
$$= \vec{d} + \vec{r},$$

with

$$\nabla \cdot \vec{d} = \nabla \cdot \vec{\xi} = \Delta D \qquad (4a)$$

$$\nabla \times \vec{r} = \nabla \times \vec{\xi} = \nabla \times (\nabla \times \vec{R}), \qquad (4b)$$

and either of the following boundary condition being satisfied:

$$\vec{n} \cdot \vec{r} = 0 \Leftrightarrow \vec{n} \cdot \nabla D = \xi_n \qquad (5a)$$

$$\vec{n} \times \vec{d} = 0 \Leftrightarrow \vec{n} \times (\nabla \times \vec{R}) = \vec{\xi}_t, \qquad (5b)$$

where $\vec{n}$ is the outward normal to the boundary. Here, $\vec{d}$ is irrotational $(\nabla \times \vec{d} = 0)$, and $\vec{r}$ is incompressible $(\nabla \cdot \vec{r} = 0)$.

We present short proofs of the decomposition's existence, orthogonality, and uniqueness for both these boundary conditions (as given in [27]).

Existence. When the *boundary condition 5a* is specified, (4a) is solved to compute $\vec{d}$. The following Poisson equation is obtained with Neumann boundary conditions:

$$\Delta D = \nabla \cdot \vec{\xi} \quad \text{on } \Omega$$
$$\nabla D \cdot \vec{n} = \xi_n \quad \text{on } \partial\Omega. \qquad (6)$$

We know that a Poisson equation with Neumann boundary conditions

$$\Delta \phi = f \qquad \text{on } \Omega$$
$$\frac{\partial \phi}{\partial \vec{n}} = g \qquad \text{on } \partial\Omega$$

has a solution unique up to an additive constant if and only if the following compatibility condition is satisfied [24]:

$$\int_\Omega f \, dV = \int_{\partial\Omega} g \, dA.$$

The additive constant can be removed by requiring that $\phi(x_0) = 0$, $x_0 \in \Omega$. Note that, the divergence theorem [41]

$$\int_\Omega \nabla \cdot \vec{\xi} \, dV = \int_{\partial\Omega} \vec{\xi} \cdot \vec{n} \, dA$$

ensures that the compatibility condition for the Poisson (6) is satisfied, hence, it has a solution D, which is unique up to a constant leading to the existence of a unique $\vec{d}(= \nabla D)$ and thus a unique $\vec{r} = \vec{\xi} - \vec{d}$.

Alternatively, if the *boundary condition 5b* is used, (4b) can be solved to compute $\vec{r}$. Since $\nabla \times (\nabla \times \vec{R}) = -\nabla^2 \vec{R}$, where ∇^2 is the vector Laplacian operator,[2] (4b) can be simplified into a vector Poisson equation with Neumann boundary condition as follows:

2. The vector laplacian of $\vec{A}$ is $\vec{\nabla}^2 \vec{A} = \nabla(\nabla \cdot \vec{A}) - \nabla \times (\nabla \times \vec{A})$. In terms of Hodge-de Rham theory, this is equal to the Laplace-de Rham operator, $\vec{\Delta} = \vec{d}\vec{\delta} + \vec{\delta}\vec{d}$.

$$\nabla^2 \vec{R} = -\nabla \times \vec{\xi} \quad \text{on } \Omega$$
$$\vec{n} \times (\nabla \times \vec{R}) = \vec{\xi}_t \quad \text{on } \partial\Omega. \qquad (7)$$

Once again, it can be shown that the Green's theorem [41] satisfies the compatibility condition for (7). Thus, it admits a solution $\vec{R}$ which is unique up to a constant leading to the existence of a unique $\vec{r} = \nabla \times \vec{R}$ and, thus, a unique $\vec{d} = \vec{\xi} - \vec{r}$.

Orthogonality. The orthogonality with respect to the L^2 inner product $(\langle f, g \rangle = \int f \cdot g)$ is established by showing that

$$\int_\Omega \vec{d} \cdot \vec{r} \, dV = 0.$$

Corresponding to the boundary conditions (5a) and (5b), respectively, it is shown that: 1) the space of gradient vector fields is orthogonal to the space of divergence-free vector fields that are parallel to the boundary, and 2) the space of divergence-free vector fields is orthogonal to the space of gradient vector fields that are normal to the boundary.

In the case of *boundary condition (5a)* $(\vec{n} \cdot \vec{r} = 0)$,

$$\int_\Omega \vec{d} \cdot \vec{r} \, dV = \int_\Omega \nabla D \cdot \vec{r} \, dV. \qquad (8)$$

By the chain rule,

$$\nabla \cdot (D\vec{r}) = \nabla D \cdot \vec{r} + D(\nabla \cdot \vec{r})$$
$$\Rightarrow \nabla \cdot (D\vec{r}) = \nabla D \cdot \vec{r} \qquad (\text{as } \nabla \cdot \vec{r} = 0). \qquad (9)$$

Substituting in (8),

$$\int_\Omega \vec{d} \cdot \vec{r} \, dV = \int_\Omega \nabla \cdot (D\vec{r}) \, dV. \qquad (10)$$

Using the divergence theorem [41] on the RHS

$$\int_\Omega \vec{d} \cdot \vec{r} \, dV = \int_{\partial\Omega} D\vec{r} \cdot \vec{n} \, dA = 0. \qquad (11)$$

In the case of *boundary condition (5b)* $(\vec{n} \times \vec{d} = 0)$,

$$\int_\Omega \vec{d} \cdot \vec{r} \, dV = \int_\Omega \vec{d} \cdot (\nabla \times \vec{R}) \, dV$$
$$= \int_\Omega \nabla \cdot (\vec{R} \times \vec{d}) \, dV.$$

Using the divergence theorem [41], and then the vector identity $\vec{A} \cdot (\vec{B} \times \vec{C}) = (\vec{A} \times \vec{B}) \cdot \vec{C}$

$$\int_\Omega \nabla \cdot (\vec{R} \times \vec{d}) \, dV = \int_{\partial\Omega} (\vec{R} \times \vec{d}) \cdot \vec{n} \, dA$$
$$= \int_{\partial\Omega} \vec{R} \cdot (\vec{d} \times \vec{n}) \, dA = 0. \qquad (12)$$

Thus, for the decomposition to be L^2-orthogonal, the boundary conditions (5a) and (5b) are both sufficient, but not necessary. The orthogonality may be established with other types of boundary conditions as well. This will be discussed in more detail in Section 5.

Uniqueness. As already discussed, the boundary conditions imposed on the decomposition determine the uniqueness. It is important to note that the two boundary conditions (5a) and (5b) may give different unique decompositions, as the harmonic component is represented

differently. Here, we show the uniqueness of the decomposition corresponding to these boundary conditions.

Assume that two different orthogonal decompositions of a vector field (with respect to *boundary condition (5a)*) exist, such that

$$\vec{\xi} = \nabla D_1 + \vec{r}_1 = \nabla D_2 + \vec{r}_2$$
$$\Leftrightarrow 0 = \vec{r}_1 - \vec{r}_2 + \nabla(D_1 - D_2). \tag{13}$$

Taking the inner product of (13) with $\vec{r}_1 - \vec{r}_2$ gives

$$0 = \int_\Omega \left(\|\vec{r}_1 - \vec{r}_2\|^2 + (\vec{r}_1 - \vec{r}_2) \cdot \nabla(D_1 - D_2) \right) dV.$$

The second term in the integral is zero as shown below

$$\int_\Omega (\vec{r}_1 - \vec{r}_2) \cdot \nabla(D_1 - D_2) \, dV$$
$$= \int_\Omega (\vec{r}_1 \cdot \nabla D_1 + \vec{r}_2 \cdot \nabla D_2 - \vec{r}_1 \cdot \nabla D_2 - \vec{r}_2 \cdot \nabla D_1) dV$$
$$= 0 - \int_\Omega (\vec{r}_1 \cdot \nabla D_2 + \vec{r}_2 \cdot \nabla D_1) \, dV \qquad \text{(by orthogon.)}$$
$$= 0 - \int_{\partial\Omega} (D_2 \vec{r}_1 \cdot \vec{n} + D_1 \vec{r}_2 \cdot \vec{n}) \, dA \qquad \text{(by (11))}$$
$$= 0 \qquad\qquad \text{(by boundary condition (5a)).}$$

Thus, the above equality is satisfied only if $\int_\Omega \|\vec{r}_1 - \vec{r}_2\|^2 \, dV = 0 \Rightarrow \vec{r}_1 = \vec{r}_2$, which implies $\nabla D_1 = \nabla D_2$ which violates the assumption. Thus, the decomposition given by the boundary condition (5a) is unique.

Similarly, by taking the inner product of (13) with $\nabla(D_1 - D_2)$, it can be shown that the decomposition given by the *boundary condition (5b)* is unique.

Intuitively, if the physical system guiding the decomposition specifies the normal component ξ_n, a unique and orthogonal decomposition can be computed using (6). In this case, any harmonic component in the field is represented within $\vec{d}$. Analogously, if the tangential component $\vec{\xi}_t$ is specified, (7) can be used to obtain a unique and orthogonal decomposition, where the harmonic component is represented within $\vec{r}$.

However, if the system can specify both ξ_n and $\vec{\xi}_t$, the harmonic component can be extracted out of both $\vec{d}$ and $\vec{r}$, and represented independently, giving rise to the three component form of the HHD.

3.3.2 HHD—Three Component Form

As discussed in Section 3.1, the harmonic field is zero in case of an infinite space. However, for domains with boundary, it can be induced by a nonzero flow on the boundary ($\vec{\xi} \neq 0$ on $\partial\Omega$). If the value of $\vec{\xi}(= \xi_n \cdot \vec{n} + \vec{\xi}_t)$ is known at the boundary, one can formulate the three component form of the decomposition as follows [97]:

Theorem 3.3 (Helmholtz-Hodge Decomposition). *A smooth vector field $\vec{\xi}$, defined on a bounded or an unbounded domain, can be uniquely decomposed into three components: 1) an irrotational component $\vec{d}$, which is normal to the boundary; 2) an incompressible component $\vec{r}$, which is parallel to the boundary; and 3) a harmonic component $\vec{h}$.*

The components $\vec{d}$ and $\vec{r}$ can be calculated as the gradient of a scalar potential (D) and the curl of a vector potential ($\vec{R}$), respectively,

$$\vec{\xi} = \nabla D + \nabla \times \vec{R} + \vec{h}$$
$$= \vec{d} + \vec{r} + \vec{h}. \tag{14}$$

In $\mathbb{R}^2$ (or a 2-manifold embedded in $\mathbb{R}^3$), curl is a scalar quantity in the upward normal direction. Hence, instead of needing a vector potential $\vec{R}$, the incompressible component can be represented using the curl of a scalar potential R to simplify the decomposition as

$$\vec{\xi} = \nabla D + J\nabla R + \vec{h}$$
$$= \vec{d} + \vec{r} + \vec{h}, \tag{15}$$

and the Poisson equations (4) become

$$\Delta D = \nabla \cdot \vec{\xi}$$
$$\Delta R = -\nabla \cdot J\vec{\xi}, \tag{16}$$

where R is a scalar potential, and the operator J rotates a 2D vector counterclockwise by $\pi/2$. Equations (15) and (16) can be derived using the properties of J. By definition, if $\vec{v} = (v_1, v_2)$, then $J\vec{v} = (-v_2, v_1)$. Now,

$$\nabla \times \vec{v} = -\nabla \cdot J\vec{v}.$$

This can be derived simply as:

$$\nabla \cdot \vec{v} = \frac{\partial v_1}{\partial x} + \frac{\partial v_2}{\partial y}$$
$$\nabla \times \vec{v} = \frac{\partial v_2}{\partial x} - \frac{\partial v_1}{\partial y} \qquad = \nabla \cdot (v_2, -v_1)$$
$$= \nabla \cdot (-J(v_1, v_2))$$
$$= -\nabla \cdot J\vec{v}.$$

Now, consider a scalar field S. Then, $J\nabla S$ is an incompressible vector field, because $\nabla \cdot J\nabla S = -\nabla \times \nabla S = 0$. Thus, instead of defining $\vec{r} = \nabla \times \vec{R}$, the incompressible component can be defined as $\vec{r} = J\nabla R$, where R is a scalar potential and avoid using the vector potential. The curl-curl equation (4b) can be simplified as follows

$$\nabla \times \vec{r} = \nabla \times \vec{\xi}$$
$$-\nabla \cdot J(\vec{r}) = -\nabla \cdot J\vec{\xi}$$
$$-\nabla \cdot J(J\nabla R) = -\nabla \cdot J\vec{\xi}$$
$$\nabla^2 R = -\nabla \cdot J\vec{\xi}.$$

For both (14) and (15), $\nabla \times \vec{d} = 0$, $\nabla \cdot \vec{r} = 0$, and $\nabla \cdot \vec{h} = 0$ and $\nabla \times \vec{h} = \vec{0}$. Under the application of both the boundary conditions $\vec{r} \cdot \vec{n} = 0$ and $\vec{d} \times \vec{n} = 0$, the proofs of existence, orthogonality, and uniqueness given in Section 3.3.1 hold.

4 APPLICATIONS

A wide spectrum of applications in various communities have used the HHD and this section discusses a representative set.

4.1 Projection Methods in Solving NSE for Incompressible Fluids

The Projection methods, introduced by Chorin [19], [20], [21], are widely used by researchers to solve the NSE for incompressible fluids. Due to its applicability in the projection methods, the HHD is one of the most important theorems in fluid dynamics.

The incompressible NSE describes the motion of fluids and are used in countless applications in science and engineering. The incompressible NSE is given as

$$\partial_t \vec{u} + (\vec{u} \cdot \nabla)\vec{u} + \frac{1}{\rho}\nabla p = \frac{\mu}{\rho}\Delta\vec{u} + \vec{F} \qquad (17a)$$

$$\nabla \cdot \vec{u} = 0, \qquad (17b)$$

where $\vec{u}$ is the velocity field of an incompressible fluid, p represents the hydrodynamic pressure, μ is the kinematic viscosity, ρ is the fluid density, and $\vec{F}$ represents any external forces. Using (17), the projection methods model the fluid motion by taking small steps in time. For each time step, the velocity from the previous time step is used to update the velocity.
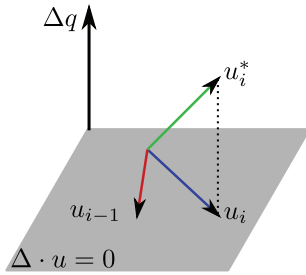
As discussed in Section 3.3.2, the space of gradient vector fields (∇q) is orthogonal to space of divergence-free vector fields ($\nabla \cdot \vec{u} = 0$) under appropriate boundary conditions. For each time step, the projection methods compute the new velocity in two substeps. In the first substep, only the momentum equation (17a) is used to compute an intermediate velocity $\vec{u}_i^*$ (green) from the divergence-free velocity, $\vec{u}_{i-1}$ (red) and pressure, p_{i-1} of the previous time step. This substep ignores the incompressibility constraint (17b). In the second substep, the intermediate velocity is projected on to the space of divergence-free vector fields using the HHD to get the get the divergence-free velocity, $\vec{u}_i$ (blue). The projection step can be written as $\vec{u} = \mathcal{P}(\vec{u}^*)$, where the projection $\mathcal{P}$ is the HHD

$$\vec{\xi} = \vec{r} + \nabla D \quad \equiv \quad \vec{r} = \mathcal{P}(\vec{\xi}).$$

The key advantage of using the HHD in this context is the decoupling of pressure and velocity fields. If the computation preserves orthogonality of the decomposition, any error in one of the terms is not reflected in the other. This procedure is more efficient than solving a coupled system of NSEs for velocity and pressure.

An immense amount of literature is available in computational physics, which deals with different techniques to enforce incompressibility in projection methods. Bell et al. [9], [10] and Stephens et al. [96] propose solutions of NSE with second order accuracy. Popinet [85] uses a solver using an octree data structure leading to an asymmetric linear system, which can be efficiently solved using multigrid methods. Min et al. [71], [72] introduce a second order accurate method to compute projection on nongraded adaptive grids. A more descriptive discussion and analysis on projection methods and their applications can be found in [15], [45], [62].

4.2 Vector Fields in Animation

Researchers in computer graphics and animation are interested in modeling and rendering fluids such as water, smoke, fire, and so on. Unlike most other areas in which most applications are primarily concerned with accuracy, graphics applications are typically more interested in real time and visually compelling animations. Such applications may choose to trade accuracy for speed.

As before, to ensure incompressibility in the fluid, a projection step using the HHD is involved as a part of the algorithm. The Eulerian formulation of the fluid simulation allows for a straightforward application of the HHD in the projection step. However, the Lagrangian formulation represents the fluid motion using the material derivative, which induces a divergence that needs to be taken into account. An excellent survey on the methods for fluid simulation is given in the book by Bridson [14].

Foster and Metaxas [34] use the Successive Over Relaxation (SOR) scheme to maintain mass-conservation property. This was the first of its kind method that solved the full 3D NSE to animate fluids. Stam [92] improves it by introducing the semi-Lagrangian method for the convection term. Fedkiw et al. [32] also use a semi-Lagrangian approach for vorticity confinement to simulate smoke with visually rich small scale rolling motion. The proposed solver removes the problems of numerical dissipation in [92]. They use a staggered grid where the fluid samples are defined on the faces of the voxels (instead of centers of the voxels as in [92]). Stam [93], Foster and Metaxas [35], Nguyen et al. [77] have been able to achieve visually compelling and near-accurate simulations and animations of fluids. Losasso et al. [64] simulate water and smoke on an octree. Maintaining the flow divergence free is the key component of the entire process, which makes the application of the HHD indispensable. A survey on the methods used for physically realistic fluid animations is given in [55], while the readers interested in photo realistic fluid rendering may refer to [82].

4.3 Vector Field Design and Analysis

Polthier and Preuß [83], [84] propose to identify the singularities in a vector field as the critical points of the potential functions of its HHD. Their global variational approach provides continuous and piecewise linear (PL) scalar potentials, which help identifying the features in the individual components ($\vec{d}$ and $\vec{r}$), respectively, which might otherwise not be visible due to overwhelming other components. This work is limited to 2D flow fields only, because 3D HHD gives a vector component and a scalar component.

Tong et al. [97] extend this technique for 3D feature identification by defining the scalar and vector potential functions on vertices of the given triangulation, while all the vector fields are defined at the center of the cells. Wiebel [101] applies this method for vortex detection by extracting

the ridge and valley lines of the magnitude field of the vector potential $\vec{R}$. Applications in computer vision and robotics employ critical point detection in various forms.

As motivated by Tong et al. [97], for complex flow fields, obtaining a multiscale representation which can highlight or obfuscate features at a user-desired scale can enhance the visualization. It is useful to be able to observe a general trend in the field, and then be able to refine the resolution to visualize smaller details. Once the HHD of the field has been calculated, the two potentials can be smoothed out and recombined to give a HHD-consistent smoother version of the vector field. As pointed out by Tong, the vector fields given by the smoothed potentials will maintain their incompressible and irrotational properties.

Wang et al. [99] followed by Fisher et al. [33] use the HHD for design of tangent vector field by placing sources and sinks at the vertices (0-forms) to define $\vec{d}$, and vortices at the faces (2-forms) to define $\vec{r}$. Then, the tangent vector field $\vec{\xi}$ is defined on edges (1-forms) by combining them using the HHD.

4.4 Computer Vision and Robotics

Recently, the field of computer vision and robotics has started exploiting the HHD. Guo et al. [43] did the seminal work in this field by decomposing the motion fields defined on regular grids using the discrete HHD proposed by Polthier and Preuß [83], [84]. They extend their work to cardiac video analysis by using a sequence of images to represent the motion [44]. Palit et al. [80] have used HHD for hurricane eye detection and fingerprints matching, and Gao et al. [38] to detect the singularities (core and delta points) in fingerprint images. Mochizuki and Imiya [73] developed algorithms to detect free space and directions to guide robot navigation, and Hatton and Choset [47] use the HHD to determine an optimum choice of coordinates for locomotive systems.

4.5 Others

The HHD has been widely used in context of a variety of other applications. In the imaging community, Hinkle et al. [52] have proposed a robust image reconstruction method to track organ motion, which applies the projection in the Fourier domain.

In the field of acoustic tomography, Johnson et al. [56] use the HHD to study velocity vector fields in blood vessels from acoustic time-offlight measurements. Norton [78], [79] derive a reconstruction method for the vector fields using the HHD in Fourier domain. These methods only deal with the incompressible component of the field. Later, Braun and Hauck [13] have shown how to compute the irrotational component, thus completing the decomposition of flow in 2D, and Prince [86] extends this work to 3D.

Georgobiani et al. [40], [67], [95] used the HHD to decompose the flow fields obtained from the simulations of solar convection to separate turbulence from acoustics, while Scharstein [87] uses the HHD to decompose the surface electric current in electromagnetic scattering problems. Miller [70] also discusses the HHD in context of classical electromagnetism. The HHD has also been used in Seismology [3], [4] for geomagnetic field modeling to approximate the solution to Maxwell's equations.

5 BOUNDARY CONDITIONS FOR THE HHD

The boundary conditions are one of the most important aspects of the decomposition. In particular, the consistency of the boundary conditions influences the orthogonality and uniqueness of the decomposition. Various researchers have experimented with the boundary conditions under general or specific settings. This section focuses on the impact of boundary conditions, and discusses a few of them found in literature.

5.1 Boundary Conditions and Orthogonality

From Section 3.3.1, we know that an L^2-orthogonal (and hence, unique) decomposition can be obtained by applying either (two-component form) or both (three-component form) of the following boundary conditions:

- $\vec{d} \times \vec{n} = 0$, i.e., the irrotational component is normal to the boundary.
- $\vec{r} \cdot \vec{n} = 0$, i.e., the incompressible component is parallel to the boundary,

where $\vec{n}$ is the outward normal to the boundary. For shorthand, these boundary conditions will be referred to as the N-P (normal-parallel) boundary conditions.

However, these conditions are only sufficient but not necessary for orthogonality. Any boundary condition that satisfies that either of the expressions (11) or (12) is zero ensures orthogonality. For example, suitable periodic boundary conditions can be applied to enforce orthogonality.

For certain specific settings, the boundary conditions can be simplified while maintaining orthogonality. For example, considering no-flow ($\xi_n = 0$ on $\partial\Omega$) or no-slip ($\vec{\xi} = 0$ on $\partial\Omega$) boundary conditions imposed on the fluid, the boundary condition (5a) translates into $\nabla D \cdot \vec{n} = 0 = \frac{\partial D}{\partial \vec{n}}$, which still guarantees the orthogonality of the decomposition. Similarly, for no-slip boundary, $\vec{r} \times \vec{n} = 0$ maintains orthogonality.

Orthogonality of vector spaces is an important property which has interested mathematicians for a long time. In 1940, Weyl [100] and in 1960, Bykhovskiy and Smirnov [16] studied orthogonality of L^2 vector spaces. Around the same time, the projection methods were developed by Chorin [19], [20] that exploited the orthogonality of the HHD for fluid modeling. Since then, they have been an integral part of fluid modeling.

If orthogonality is not required, the decomposition can take various forms depending upon the boundary conditions. More general, HHD-like nonorthogonal decompositions, $\vec{\xi} = \nabla D + \nabla \times \vec{R}$, and their existence and uniqueness properties under different boundary conditions on D or $\vec{R}$ have been studied, e.g., [5], [8].

However, Weinan and Liu [31] comment that the choice of boundary conditions of projection methods is controversial and raised the question *"whether orthogonality is really important?"* They consider the effect of numerical application of boundary conditions on the boundary layer structure. Denaro [27] followed up with a numerical validation and comparison of orthogonal and nonorthogonal decompositions and concluded that *"orthogonality of the decomposition should be always maintained for all the flow problems of practical interest."*

5.2 Harmonic Field and the Topology of the Domain

So far, we have concentrated on simply connected domains with boundary, and showed that a harmonic component is obtained by applying varying boundary conditions. Section 3.1 argues that this harmonic component can be represented as gradient of a scalar function, or the curl of a vector function.

However, for more general (nonsimply connected) domains, this harmonic component $\vec{h}$ in the HHD can be further split by applying boundary conditions:

$$\vec{h} = \nabla H_s + \vec{h_1} \ \left(\vec{h_1} \cdot \vec{n} = 0 \text{ at } \partial\Omega \right) \tag{18a}$$

$$\vec{h} = \nabla \times \vec{H_v} + \vec{h_2} \ \left(\vec{h_2} \times \vec{n} = 0 \text{ at } \partial\Omega \right). \tag{18b}$$

Such a decomposition is often referred to as the *Hodge-Morrey-Friedrichs Decomposition (HMFD)*. Note that the HMFD is a general form of the HHD, and is always valid. However, for simply connected domains, $\vec{h_1} = \vec{h_2} = 0$, and hence it reduces to HHD. For more details on general forms of HHD, the reader may refer to Schwarz [89].

5.3 HHD Boundary Conditions in Projection Methods

When computing projection methods for fluid modeling using NSE, scientists are interested in experimenting with new models of flow, in terms of spatial and/or temporal discretization, and boundary conditions. There exists rich literature in the communities of fluid modeling, computational physics, and numerical methods that investigates the accuracy and convergence of such models. While their prime objective is to provide better approximations to the solution of NSE, the HHD forms a smaller, yet, an integral part of the entire process. The discretization methods and the boundary conditions of the system as a whole have a strong influence on their choice of boundary conditions in the projection step.

For example, consider the modeling of a fluid (water, smoke, and so on) bounded by air. Air, being lighter than the modeled fluids, is assumed to have only a small effect on the fluid. Since the entire atmosphere cannot be modeled, only an interesting region of the space is modeled, and the fluid is free to enter or exit the domain. This kind of boundary is called the *free* boundary, and is modeled by setting the pressure to zero at the boundary. Note that, $p = 0$ leads to ∇p being normal to the boundary, and the orthogonality is respected.

There exist two approaches to compute the projection: 1) the gradient component (∇D) can be computed, and then the divergence-free component is given as $\vec{r} = \vec{\xi} - \nabla D$, as done by Chorin [19], [20], [21] and van Kan [98]; and 2) the divergence-free component can be directly solved for, as done by Bell, Stephens and others [9], [10], [96]. Depending upon the type of discretization chosen for either of these approaches, one may make a choice for boundary conditions that improve accuracy. For example, the MAC grid [46] used in finite volume methods, where the pressure is stored at the cells centers and the velocity components are stored at their respective cells faces, is common, because it offers a straightforward mechanism to enforce the incompressibility discretely. However, other arrangements have been shown to produce higher order accurate schemes for
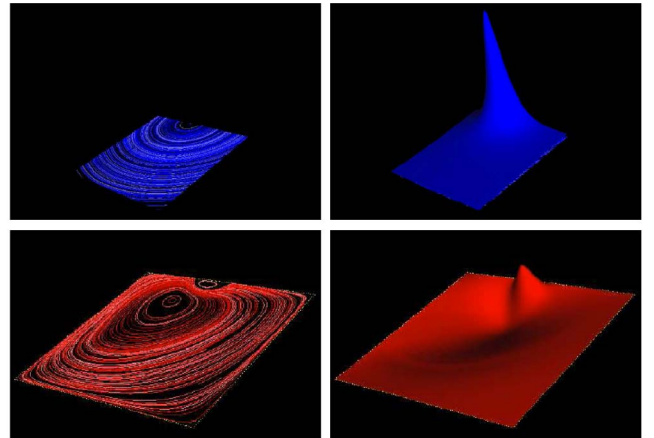

Fig. 2. Example given by Wiebel [101] to show drawbacks of the HHD. Top: The original vector field (left) and potential function (right). Bottom: The recovered vector field (left) and potential function (right) after HHD. After recombination the rotation is inverted and an additional critical point is introduced.

the velocity field, without enforcing the incompressibility condition at the discrete level (e.g., [15], [31]).

To maintain the focus of this survey, we do not delve into the numerous technical details of the choice of boundary conditions in projection methods, because they do not pertain to our discussion on the HHD. Irrespective of the choice of boundary conditions for the projection step, however, the orthogonality of the decomposition is always desirable.

5.4 HHD Boundary Conditions in Flow Analysis and Visualization

In topological analysis and flow visualization, orthogonality might be desirable for obtaining a unique decomposition. Since there are no boundary conditions superimposed by the fluid model, the treatment of the issue is less involving. Polthier and Preuß [83], [84] as well as Tong et al. [97] enforce the *N-P* boundary conditions for the extraction of all the three components of the HHD.

Guo et al. [42], [43] and others extending these ideas (see Fig. 1), however, do not specify any boundary conditions. According to [42], [43], setting the potentials zero at only one vertex is sufficient to compute the decomposition uniquely, although, they do not make any claims about the orthogonality of the decomposition. For better accuracy in results, they propose to further decompose the harmonic component recursively. The need for a recursive solution remains unclear, because with consistent boundary conditions there should exist a unique solution up to numerical precision, which can be computed directly as in the methods of Polthier and Tong. In Guo's case, this seems to be due to the lack of proper boundary conditions, because as discussed in Section 3, the correct boundary conditions must be specified to obtain a unique decomposition. The technical details of Guo's work will be discussed in Section 6.1.3.

Wiebel [101] also implements and uses Polthier's algorithm for the 2D discrete HHD. He provides an example of an incompressible vector field rotating counterclockwise with the center of the rotation lying on the boundary. Fig. 2 shows his example along with the corresponding potential
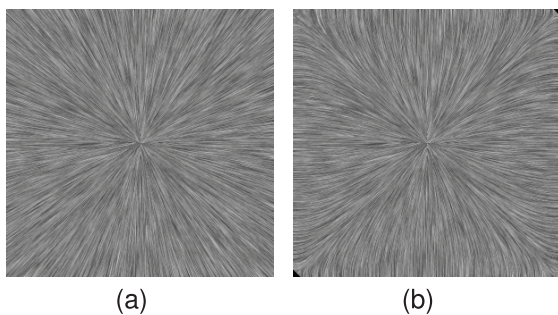
(a)   (b)

Fig. 3. An example to show artifacts of *N-P* boundary conditions. (a) The original vector field $(\vec{V}(x,y) = (x,y))$. (b) The irrotational component $(\vec{d})$ recovered after HHD. Artifacts are seen near the boundary because the *N-P* boundary conditions enforce the flow to be normal to the boundary. The incompressible component $\vec{r}$ is zero for this example, while the harmonic component $\vec{h}$ also shows similar artifacts due to residual.

function of the rotational component having a maximum at the boundary. As shown in the figure, decomposing this field results in an entirely different vector field in which the rotation is clockwise for most of the domain. Examining the corresponding potential function shows that a new minimum is introduced near the boundary, while the magnitude of the original maximum is reduced. Wiebel notes this as a drawback of the decomposition.

This can, however, be explained in terms of the boundary conditions. Suppose the original vector field is purely irrotational, and the flow on the boundary is distributed arbitrarily (not necessarily normal everywhere on the boundary). One such example is the vector field defined by a nodal source at the origin of a square domain, as shown in Fig. 3. If the HHD is computed for this vector field, the incompressible component will be zero. However, in light of boundary conditions $\vec{d} \perp \vec{n} = 0$, it can be easily observed that at the boundary, a disagreement occurs between the original vector field and the boundary conditions. The manifestations of such disagreements are stronger when the critical point lies closer to the boundary. Thus, these artifacts are the by-product of the boundary conditions, and are admitted in the solution to obtain a unique and orthogonal decomposition.

In a recent paper, Petronetto et al. [81] compute the 2D HHD with a different set of boundary conditions, which are opposite to the *N-P* boundary conditions. According to them, these boundary conditions are the usual boundary conditions for the decomposition. For shorthand, these boundary conditions will be referred to as the *P-N*

(parallel—normal) boundary conditions. According to the *P-N* boundary conditions,

- $\vec{d} \cdot \vec{n} = 0$, i.e., the irrotational component is parallel to the boundary.
- $\vec{r} \times \vec{n} = 0$, i.e., the incompressible component is normal to the boundary.

Petronetto draws inspiration from Colin et al. [23] who compute the divergence-free flow from a given flow using the projection. Without citing any literature, Colin uses the Neumann boundary conditions $\frac{\partial D}{\partial n} = 0$ for boundaries, which are neither no flow, nor no slip. As it has already been discussed, $\frac{\partial D}{\partial n} = 0$ satisfies orthogonality only when no-slip or no-flow boundary is in place, i.e., $\xi_n = 0$. As we show in [11], the *P-N* boundary conditions are, in general, invalid, and cannot be used to compute the HHD of a general vector field. Thus, there is a discrepancy in the understanding of the boundary conditions of HHD, which needs to be illuminated.

6 TECHNIQUES FOR HHD COMPUTATION

This section will briefly introduce the most common methods to compute the discrete HHD developed in various communities. The aim is to provide the reader with a general overview of potential techniques and references to the relevant papers.

The majority of techniques using the HHD do so incidentally as part of a projection method for fluid modeling. Here, we briefly discuss the different approaches of computing the projection and provide a more detailed discussion on techniques designed specifically to compute the HHD. The primary focus will be the discretization of the necessary differential operators and the different boundary conditions but where available the numerical performance is discussed as well. Table 2 summarizes these techniques to allow an easy comparison.

6.1 Least Squares Finite Elements Method (LS-FEM)

Many of the recent techniques to compute the discrete HHD employ a variational approach where certain energy functionals, created using finite element approach, are minimized to compute the irrotational and incompressible components. These techniques work for piecewise constant (PC) vector fields (defined on the triangles of the mesh), resulting in PL potential functions (defined on the vertices of the mesh) after the decomposition.

TABLE 2
A Comparative Summary of Techniques for HHD Computation

Section: Technique	Domain	Bound. Cond.	L_2-ortho.	Coherence	References
6.1: Least Squares Finite Elements Method (LS-FEM)	tri/tet mesh	N-P	$O(10^{-2})^\dagger$	$O(10^{-2})^\dagger$	[83], [84]
6.2: Smoothed Particle Hydrodynamics (SPH)	particles	N-P, P-N	$O(10^{-2})$	$O(10^{-5})$	[81]
6.3: Finite Difference Methods (FDM)	regular grid	no flow $\left(\vec{\xi} \cdot \vec{n} = 0\right)$	$O(\Delta t)^*$	$O(\Delta t^3)^*$	[9]
6.4: Fourier & Wavelets Domains	regular grid	fixed/periodic $\left(\vec{\xi} \cdot \vec{n} = 0\right)$	-	$O(10^{-2})$	[28]
6.5: Statistical Learning using Matrix-Valued Kernels	particles	-	-	$O(10^{-1})$	[66]

For each category, the required domain and the applicable boundary conditions are given. Coherence measures the amount of divergence and curl in the obtained components, and L_2 ortho. measures the error in orthogonality of the obtained components. (†: The numbers are taken from our implementation of [84]. The original publication does not provide a numerical analysis. *: Δt is the time discretization step size.)
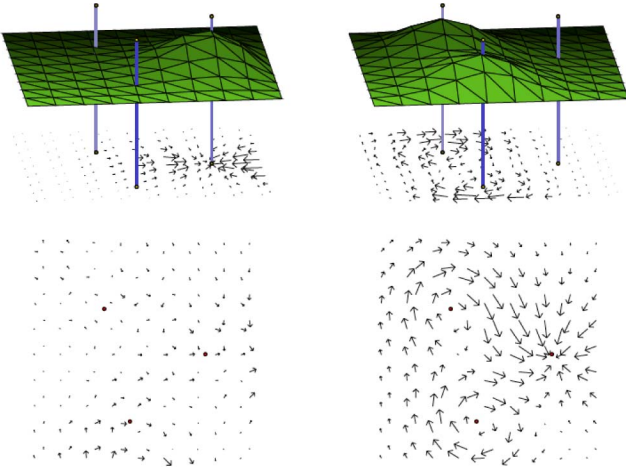
Fig. 4. Results provided by Polthier and Preuß [84]. Top left to bottom right: The irrotational component, $\vec{d}$, with scalar potential D, the incompressible component, $\vec{r}$, with scalar potential R, the harmonic component ($\vec{h}$), and the original vector field ($\vec{\xi}$).

6.1.1 HHD for 2D Triangular Meshes Using LS-FEM

Polthier and Preuß [84] provide definitions for the discrete divergence and discrete rotation on a 2-manifold similar to weak derivatives in the finite element methods, and use them to propose a simple implementation of the discrete HHD. The 2D HHD (15) is computed by solving the Poisson equation (16) using a variational approach, where energy functionals are minimized for the irrotational and incompressible components. Finally, the harmonic component is computed as the residual and thus is less accurate, because the error caused due to the approximation or the boundary conditions are reflected in the residual.

The discrete divergence and discrete rotation for a PC vector field are defined as PL scalar functions. McCormick [68] discusses in detail the finite-element approach using primal potential and dual vector fields. In the following, let $\mathbb{S}(p)$ denote the star of the vertex p:

1. *Discrete Divergence* $(\nabla \cdot \vec{\xi})$: For a vertex p, the discrete divergence can be defined as the net flow normal to the boundary of $\mathbb{S}(p)$. It can be calculated as the integrated dot product of the vector with the outward normal for every triangle in $\mathbb{S}(p)$. The outward normal can also be calculated by rotating the normalized edge vector $\vec{c}$ (of the triangles in $\mathbb{S}(p)$), which does not have p as one of its vertices

$$\nabla \cdot \vec{\xi}(p) = \sum_{i=1}^{k} \langle \vec{\xi}_i \nabla \phi_{p_i} \rangle = -\frac{1}{2} \sum_{i=1}^{k} \langle \vec{\xi}_i J \vec{c}_{p_i} \rangle$$

where k is the number of triangles in $\mathbb{S}(p)$, $\nabla \phi_p$ is the Lagrange basis function corresponding to vertex p, and J rotates a vector counterclockwise by $\pi/2$ degrees.

2. *Discrete Rotation* $(\nabla \times \vec{\xi})$: For a vertex p, the discrete rotation can be defined as the net flow tangential to the boundary of $\mathbb{S}(p)$. It can be calculated as the integrated dot product of the vector with the rotated outward normal for every triangle in $\mathbb{S}(p)$. The rotated outward normal is same as the normalized edge vector $\vec{c}$ in $\mathbb{S}(p)$

$$\nabla \times \vec{\xi}(p) = -\sum_{i=1}^{k} \langle J\vec{\xi}_i, \nabla \phi_{p_i} \rangle = \frac{1}{2} \sum_{i=1}^{k} \langle \vec{\xi}_i \vec{c}_{p_i} \rangle.$$

The two energy functionals are given by

$$F(D) = \int \left(\vec{\xi} - \nabla D \right)^2$$
$$= \int \left(|\nabla D|^2 - 2\langle \nabla D, \vec{\xi} \rangle \right) + \int |\vec{\xi}|^2$$
$$G(R) = \int \left(\vec{\xi} - J\nabla R \right)^2$$
$$= \int \left(|J\nabla R|^2 - 2\langle J\nabla R \vec{\xi} \rangle \right) + \int |\vec{\xi}|^2.$$

To achieve these minimizations, the derivatives of both the functionals should vanish at every vertex. Explicit representations of the derivatives at p are given by

$$\frac{d}{dD_p} F(D) = -\sum_{i=1}^{k} \left\langle \left(\nabla D_i - \vec{\xi} \right), J\vec{c}_{p_i} \right\rangle = 0$$
$$\frac{d}{dR_p} G(R) = \sum_{i=1}^{k} \left\langle \left(\nabla R_i + J\vec{\xi} \right), J\vec{c}_{p_i} \right\rangle = 0. \tag{19}$$

Once the irrotational and incompressible components have been computed, the harmonic component is found as the residual, i.e., $\vec{h} = \vec{\xi} - \nabla D - J\,\nabla R$.

The *N-P* boundary conditions are used to get the unique decomposition. Fig. 4 shows the results of HHD as presented in [84]. Note that no numerical analysis of the technique is given in [84], and Table 2 shows the analysis of our implementation of this technique.

6.1.2 HHD for 3D Tetrahedral Meshes Using LS-FEM

Tong et al. [97] extend Polthier's method [84] to 3D by defining the discrete divergence, discrete curl, and minimizing the energy functionals for PC vector fields on a tetrahedral mesh. Like the previous method, the potentials D and $\vec{R}$ are defined per-vertex (PL), but here in 3D, the incompressible component needs a vector potential $\vec{R}$. After defining the decomposition for 3D fields, Tong et al. define a multiscale model to compute the decomposition. The discrete operators used are:

1. *Discrete Divergence* $(\nabla \cdot \vec{\xi})$: For a vertex p, the discrete divergence can be defined as

$$\nabla \cdot \vec{\xi}(p) = \sum_{i=1}^{k} \langle \nabla \phi_{p_i}, \vec{\xi}_i |T_i| \rangle$$

where k is the number of tetrahedra in $\mathbb{S}(p)$, $|T_i|$ is the volume of the tetrahedron T_i, and for implementation purposes, $\nabla \phi_{p_i}$ is the normal vector to the face f_{pi} opposite to p in T_i, pointing toward i, with magnitude of $\|\nabla \phi_{p_i}\| = \frac{area(f_{ik})}{2|T_k|}$.

2. *Discrete Curl* $(\nabla \times \vec{\xi})$: For a vertex p, the discrete curl can be defined as

$$\nabla \times \vec{\xi}(p) = \sum_{i=1}^{k} \langle (\nabla \phi_{p_i} \times \vec{\xi}_i) |T_i| \rangle$$

where the symbols are same as defined above.

Fig. 5. Two-dimensional results provided by Tong et al. [97]. L-R: The original field, $\vec{\xi}$, irrotational ($\vec{d}$), and incompressible ($\vec{r}$) components. The divergence and rotation in critical points in $\vec{\xi}$ are shown in yellow.

Once again, the two potentials can be calculated by minimizing the quadratic functions corresponding to the two Poisson equations (6) and (7)

$$F(D) = \int \left(\vec{\xi} - \nabla D\right)^2$$
$$G(\vec{R}) = \int \left(\vec{\xi} - \nabla \times \vec{R}\right)^2.$$

Explicit representations of the derived linear systems are given as

$$\sum_{i=1}^{k} \nabla\phi_{p_i} \cdot (\nabla D_i)|T_i| = \sum_{i=1}^{k} \nabla\phi_{p_i} \cdot \vec{\xi}_i |T_i|$$
$$\sum_{i=1}^{k} \nabla\phi_{p_i} \times (\nabla \times \vec{R}_i)|T_i| = \sum_{i=1}^{k} \nabla\phi_{p_i} \times \vec{\xi}_i |T_i|.$$

Similar to [84], the harmonic component is found as a residual. Also, the same (N-P) boundary conditions are used. Fig. 5 shows the results of HHD as presented in [97].

6.1.3 HHD for 2D Regular Grid Data using LS-FEM

Guo et al. [43] formulate a simpler implementation of the HHD for their applications of motion fields extracted from image sequences. Since the image sequences are based on regular grids, they argue the need for a simpler implementation for decomposition.

To use the setup proposed by Polthier and Preuß [84], the vector field data on a regular grid is converted into a PC vector field on a triangulation by converting the regular grid into a regular triangulation, and assigning each triangle, the average of the vector values at its vertices. Then, the linear systems representing (19) is derived and solved for the potentials. Working with triangulation derived from regular grids reduces the computational complexity because the area of every triangle is same, hence can be computed once. Also the matrices representing the linear systems only depend on the grid size and, thus, typically need to be created only once.

However, no boundary conditions are specified in their solver, which may explain some of the artifacts in their results (see Fig. 6). Guo's MS thesis [42] explains in more detail that if the potential functions (D and R) are set to zero on the boundary, the rank of the matrices they create becomes small, and their derivation breaks. Instead, they set $D_1 = 0$ and $R_1 = 0$ and argue that this is sufficient to obtain a unique decomposition. That is, enforcing the potentials to be zero on just a single vertex results a unique solution. However, they provide no discussion on whether the
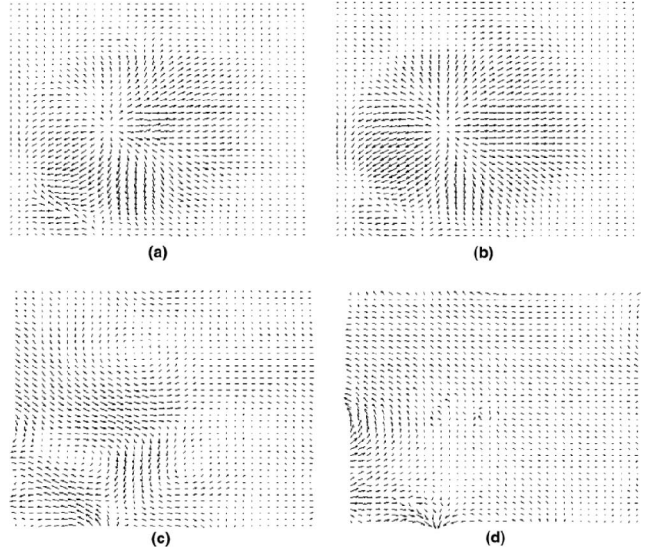

Fig. 6. Results provided by Guo et al. [43]. The figure shows (a) cardiac motion field ($\vec{\xi}$), (b) irrotational ($\vec{d}$), (c) incompressible ($\vec{r}$) and (d) harmonic ($\vec{h}$) components.

resulting decomposition is orthogonal, which casts some doubt on the uniqueness.

For better accuracy in results, they propose to further decompose the harmonic component recursively

$$\begin{aligned}
\vec{\xi} &= \vec{d}_1 + \vec{r}_1 + \vec{h}_1 \\
&= \vec{d}_1 + \vec{r}_1 + \left(\vec{d}_2 + \vec{r}_2 + \vec{h}_2\right) \\
&= \vec{d}_1 + \vec{r}_1 + \left(\vec{d}_2 + \vec{r}_2 + \left(\cdots\cdots\cdots + \vec{d}_n + \vec{r}_n + \vec{h}_n\right)\right) \\
&= \left(\vec{d}_1 + \vec{d}_2 + \cdots\vec{d}_n\right) + \left(\vec{r}_1 + \vec{r}_2 + \cdots\vec{r}_n\right) + \vec{h}_n \\
&= \vec{d} + \vec{r} + \vec{h}_n.
\end{aligned}$$

Unfortunately, the need for a recursive algorithm remains unclear because if there exists a unique solution, it should be obtained after the first solve as in previous techniques [84], [97].

6.2 Smoothed Particle Hydrodynamics (SPH)

Smoothed Particle Hydrodynamics is a computational method used for simulating fluid flows. Although originally designed for the simulations of astrophysical problems [65], SPH has been successfully used in the graphics community for fluid simulations [94]. Since it is a meshfree approximation for particle systems based on the Lagrangian description, it overcomes any mesh artifacts caused due to a Eulerian approach. SPH reduces the complexity of the simulation, by making the mass conservation equations and convection terms dispensable. For a detailed discussion on SPH, the reader may refer to [74].

The SPH approximation models a set of particles in space carrying individual physical attributes. These attributes or functions can be estimated for a particle at point $\vec{x}$ using a smoothing kernel W to approximate in a local neighborhood within distance h as follows:

$$f(\vec{x}_i) = \sum_{j \in N_i} \frac{m_j}{\rho_j} f(\vec{x}_j) W(\vec{x}_i - \vec{x}_j, h),$$
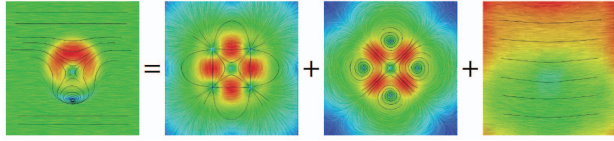
(a) L-R: The original vector field $(\vec{\xi})$, the irrotational $(\vec{d})$, incompressible $(\vec{r})$ and harmonic $(\vec{h})$ components.
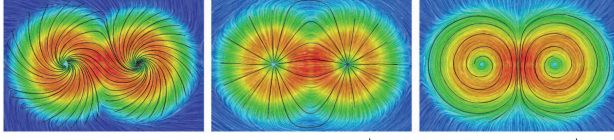
(b) L-R: The original vector field $(\vec{\xi})$, the irrotational $(\vec{d})$ and incompressible $(\vec{r})$ components.

Fig. 7. Results provided by Petronetto et al. [81]. Decomposition using (a) *N-P*, and (b) *P-N* boundary conditions. The vector magnitudes have been mapped to color to enhance the visualization.

where m_j is the mass, $\vec{x}_j$ is the position, ρ_j is the density and f_j is the quantity f for the neighboring particle j, and N_i is the set of neighboring particles with $|\vec{x}_i - \vec{x}_j| \leq h$. Using SPH, the derivatives of a function f can be obtained by using the derivatives of the smoothing kernel.

6.2.1 HHD for 2D Vector Fields using SPH

Colin et al. [23] presented an SPH solution of HHD to achieve a divergence-free vector field in an incompressible fluid simulation. The choice of approximations of the differential operators made in [23] are as follows:

$$\nabla f_i = \left(\frac{1}{\rho_i}\right) \sum_{j \in N_i} m_j (f_j - f_i) \nabla W(\vec{x}_i - \vec{x}_j, h)$$

$$(\nabla \cdot \vec{f})_i = \left(\frac{1}{\rho_i}\right) \sum_{j \in N_i} m_j (\vec{f}_j - \vec{f}_i) \cdot \nabla W(\vec{x}_i - \vec{x}_j, h)$$

$$(\Delta f)_i = \left(\frac{1}{\rho_i}\right) \sum_{j \in N_i} m_j \{ (f_i - f_j) \Delta W(\vec{x}_i - \vec{x}_j, h) - \frac{2}{\rho_i} \Delta W(\vec{x}_i - \vec{x}_j, h) \cdot \nabla \rho_j \}.$$

Using these approximations, the Poisson equations (15) are solved with Neumann boundary conditions $\frac{\partial D}{\partial \vec{n}} = \vec{d} \cdot \vec{n} = 0$.

Using a similar SPH approach, Petronetto et al. [81] present results of HHD in 2D by calculating the irrotational and harmonic components as well. Their approximation of the differential operators is given below:

$$\nabla f_i = \sum_{j \in N_i} \frac{m_j}{\rho_j} (f_j - f_i) \nabla W(\vec{x}_i - \vec{x}_j, h)$$

$$(\nabla \cdot \vec{f})_i = \sum_{j \in N_i} \frac{m_j}{\rho_j} (\vec{f}_j - \vec{f}_i) \nabla W(\vec{x}_i - \vec{x}_j, h)$$

$$(\Delta f)_i = \sum_{j \in N_i} 2 \frac{m_j (f_j - f_i)}{\rho_j \|\vec{x}_{ij}\|^2} \vec{x}_{ij} \nabla W(\vec{x}_i - \vec{x}_j, h),$$

where $\vec{x}_{ij} = \vec{x}_i - \vec{x}_j$, and W is a quartic smoothing kernel for a given value of h. The decomposition can be found by using the SPH approximations for Poisson equation for 2D (16) using the SPH approximations for Laplacian defined above. The authors provide results for both *N-P* and *P-N* boundary conditions (Fig. 7).

6.2.2 Discussion on SPH HHD Boundary Conditions

Both [23] and [81] present results for the *P-N* boundary conditions in addition to the usual *N-P* boundary conditions. The *P-N* boundary conditions can be enforced by ensuring that $\frac{\partial D}{\partial \vec{n}} = \nabla D \cdot \vec{n} = 0 = \nabla R \cdot \vec{n} = \frac{\partial R}{\partial \vec{n}}$.

Both [23] and [81] consider the usual boundary conditions for HHD to be the *P-N* boundary condition; however, no literature is cited to corroborate this statement.

In [11], we present a simple analytical example to show that the *P-N* boundary conditions are not valid in general, and can be used only if the global divergence and the global curl of the field is zero. An earlier article on SPH projection method [26] acknowledges that the Poisson equation must satisfy a compatibility constraint to ensure unique solution. In their explanation, they mention that the condition $\int_\Omega \nabla \cdot \vec{d} \, dV = \int_{\partial \Omega} \vec{d} \cdot \vec{n} \, dA = 0$ must be accompanied by a condition that the sum of the discrete source terms $(\sum_{i=1}^{N} \nabla \cdot \vec{\xi})$ must be zero. In the absence of any constraint (like $\int_\Omega \nabla \cdot \vec{\xi} = 0$), these boundary conditions are invalid and may make the convergence of the solver extremely difficult. In our implementation of 2D HHD using the LS-FEM method (Section 6.1.1), we have found that the energy minimization using the *P-N* boundary conditions does not converge.

6.3 Finite Difference Methods (FDM)

The FDM are commonly used to numerically approximate differential operators for solving differential equations. They have also been used in the projection methods for solving Poisson equation (4) for solutions of incompressible fluid simulations.

Foster and Metaxas [35] propose a finite difference approximation scheme for voxel-based fluid simulations. The scalar potential D at every vertex (represented by indices i, j, k) is calculated for each time step $h + 1$ as follows:

$$D_{i,j,k}^{h+1} = \frac{2}{8/\Delta \tau^2} \bigg\{ - (\nabla \cdot \vec{\xi})_{i,j,k} + \frac{1}{\Delta \tau^2} \Big[D_{i+1,j,k}^h + D_{i-1,j,k}^h + D_{i,j+1,k}^h + D_{i,j-1,k}^h + D_{i,j,k+1}^h + D_{i,j,k-1}^h \Big] \bigg\} - D_{i,j,k}^h.$$

The divergence operator is defined as follows:

$$(\nabla \cdot \vec{\xi})_{i,j,k} = \frac{1}{\Delta \tau} \big[\xi_{x(i_+,j,k)} - \xi_{x(i_-,j,k)} + \xi_{y(i,j_+,k)} - \xi_{y(i,j_-,k)} + \xi_{z(i,j,k_+)} - \xi_{z(i,j,k_-)} \big],$$

where i_+ and i_- represent the positions $i + 1/2$ and $i - 1/2$, respectively. Once again, no-flow boundary conditions are used, i.e., $\vec{\xi} \cdot \vec{n} = 0 = \vec{d} \cdot \vec{n}$. As discussed in Section 6.4, Hinkle et al. [52] also use a finite difference approach to approximate the DFT of the divergence of the vector field.

6.3.1 Galerkin Formulation Using Finite Differences

Building upon a Galerkin formulation of projection methods proposed by Stephens et al. [96], Bell et al. [9] propose a second-order projection method for the incompressible NSE for fluids defined on 2D regular grid cells. The Galerkin formulation refers to a class of methods for approximating the discrete counterparts of continuous differential operators used in differential

equations by defining a basis of a vector space of functions.

The unknown velocity is defined cell centered at the interior of the cells, and at the midpoints of cell edges for the boundary cells. The scalars (potential and divergence) are defined at the corners of the grid cells. Then, the gradient operator (∇) is defined as follows:

$$(\nabla D)_{x,ij} = \frac{1}{2\Delta x}\left(D_{i_+,j_+} - D_{i_-,j_+} + D_{i_+,j_-} - D_{i_-,j_-}\right)$$

$$(\nabla D)_{y,ij} = \frac{1}{2\Delta y}\left(D_{i_+,j_+} - D_{i_+,j_-} + D_{i_-,j_+} - D_{i_-,j_-}\right),$$

where (i, j) are the positional coordinates of the cells in the grid, and i_+ and i_- represent the positions $i + 1/2$ and $i - 1/2$, respectively. The divergence operator ($\nabla \cdot$) can be derived from the discrete form of integration by parts, which is

$$(\nabla \cdot \vec{\xi}, D)_s = -(\vec{\xi}, \nabla D)_v,$$

where $(,)_s$ and $(,)_v$ are the inner products defined on the discrete scalar and vector spaces, respectively. This condition also guarantees that the projection is orthogonal. These discrete differential operators are then used to define a basis ψ such that

$$\psi_{i_+,j_+} = -J\nabla D_{i_+,j_+}.$$

Finally, the divergence-free velocity $\vec{r}$ can be computed as a linear combination of the basis functions, where the weights αs are chosen such that

$$\left(\sum \alpha_{i_+,j_+}\psi_{i_+,j_+}, \psi_{k_+,l_+}\right)_v = \left(\vec{\xi}, \psi_{k_+,l_+}\right)_v.$$

A number of other variants of Galerkin formulations have been proposed for the NSE. However, the approximation for the projection steps remains largely similar with slight modifications to the discrete differential operators. For example, Bell and Marcus [10] extend the approximations of [9] for variable density flows. A similar Galerkin approach was used by Solomon and Szymczak [90], and Ingber and Kempka [54].

6.4 Fourier and Wavelets Domains

Stam [92], [93] and Hinkle et al. [52] make use of the Fourier domain to compute the divergence-free component of vector fields for fluid simulation and 4D image reconstruction, respectively. To compute the Discrete Fourier Transform (DFT) of a d-dimensional vector field, the Fourier transform of d components of the vector field are computed independently. If $\vec{v}$ is a d-dimensional vector $\vec{v} = \{v_j\}_{j=0 \ to \ d}$, then

$$\mathrm{DFT}\{\vec{v}\}\,(\omega) = \{DFT\{v_j\}(\omega)\}_{j=0 \ to \ d}.$$

Computing mass conserving and gradient vector fields is simple in Fourier domain because differentiation in the spatial domain is equivalent to multiplication by the wavenumber in the Fourier domain

$$\mathrm{DFT}\{\nabla\vec{v}\}(\omega) = \vec{k} \cdot \mathrm{DFT}\{\vec{v}\}(\omega).$$

Stam [92] introduces an unconditionally stable algorithm for modeling real-time fluid motion, which is based on a combination of a semi-Lagrangian Scheme [25] and implicit solvers to solve the NSE. As compared to [35] where stability of the model is dependent upon the step size of the integration scheme, this method is stable even for larger step sizes. He also suggests that it is more accurate than [35]. The flow is defined at the center of the cells of a regular grid, and the boundary is assumed to be fixed or periodic. For either case, no flow is allowed to cross the boundary (no flow), i.e., $\vec{\xi} \cdot \vec{n} = 0$. As a result of these boundary conditions, the harmonic component in the HHD vanishes. Furthermore, the system focuses on real time visually consistent simulations rather than numerically accurate simulations. The last step of their 4-step system is the projection or the HHD, and is calculated as a part of a Fast Fourier Transform (FFT) of the system. The projection step solves the Poisson equation (4a), with Neumann boundary condition $\frac{\partial D}{\partial \vec{n}} = 0$ because $\vec{\xi} \cdot \vec{n} = 0$. The FFT system is solved using the library FISHPAK.

Based on [92], Stam [93] presents another algorithm to compute the velocity of mass-conserving fluids using FFTs. The solver works for regular grid data, however, is specialized for domains with periodic boundary, i.e., the d-dimensional grid is assumed to be a torus. Once again, the solver sacrifices accuracy for speed and stability.

A slightly different approach is used by Hinkle et al. [52], where the DFT of the divergence of a vector field ($\nabla \cdot \vec{v}$) is computed using the discrete finite-difference derivative

$$\mathrm{DFT}\{\nabla \cdot \vec{v}\}(\omega) = W(\omega) \cdot \mathrm{DFT}\{\vec{v}\}(\omega),$$

where

$$W(\omega) = \frac{i}{2}\begin{pmatrix} \frac{1}{h_x}\sin\frac{\omega_x}{N_x} \\ \frac{1}{h_y}\sin\frac{\omega_y}{N_y} \\ \frac{1}{h_z}\sin\frac{\omega_z}{N_z} \end{pmatrix}.$$

Here, $i = \sqrt{-1}$, and N and h are the number of samples in grid and the spacing between adjacent grid points, respectively, given component wise in x, y, z directions.

Using this definition, the projection step to compute the mass-conserving vector field $\vec{r}$ can be performed as

$$\mathrm{DFT}\{\vec{r}\}(\omega) = \mathrm{DFT}\{\xi\}(\omega) - \frac{W(\omega) \cdot \mathrm{DFT}\{\vec{\xi}\}(\omega)}{\|W(\omega)\|_{\mathbb{C}^3}^2}W(\omega).$$

Deriaz and Perrier [28], [29], [30] propose an iterative algorithm to compute the HHD in wavelet domain. Due to the localized nature of wavelets in both physical and frequency domains, such a decomposition is localized in physical space as compared to the decomposition in Fourier domain. They provide a basis for 2D and 3D decompositions which is generalizable to arbitrary dimension, and is extendable to nonperiodic boundaries.

6.5 Statistical Learning Using Matrix-Valued Kernels

Macêdo and Castro [66] propose using sparse, unstructured, and possibly noisy samples of a vector field, to
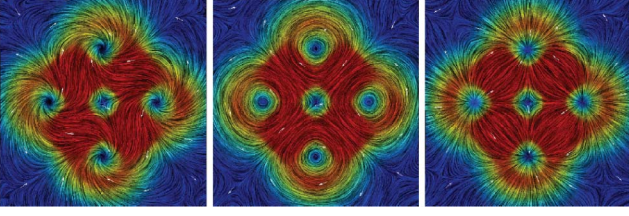
Fig. 8. Results provided by Macêdo and Castro [66]. From left to right: The original field, the learned divergence-free component, and the learned curl-free component.

construct its incompressible and irrotational components using matrix-valued radial basis function (RBF) kernels. A vector field can be learned as linear combination of a kernel. $\vec{V}(x) = \sum_{i=1}^{N} K(x, x^i)(\alpha^i - \alpha^{*i})$, where the weights $(\alpha - \alpha^*)$ are computed by optimizing a loss function [69]. The problem then reduces to finding the appropriate kernels.

According to Narcowich and Ward [76] and Fuselier [37], the matrix-valued divergence-free and curl-free kernels can be obtained from the divergence-free and curl-free matrix-valued RBFs as $K(x, x') = \Phi(x - x')$, such that

$$\Phi_{df}(x) = H\phi(x) - tr\{H\phi(x)\}I$$
$$\Phi_{cf}(x) = -H\phi(x),$$

where ϕ is a scalar-valued RBF, H is the Hessian operator, such that $(H\phi)_{ij} = \frac{\partial^2\phi}{\partial x_i \partial x_j}$, and I is the identity matrix. It can be verified that the columns of Φ_{df} and Φ_{cf} are divergence-free and curl-free, respectively.

According to Macêdo and Castro [66], it is possible to consider a convex linear combination of the kernels K_{df} and K_{cf} to obtain a kernel for learning any kind of vector field. More importantly, this allows to reconstruct the divergence-free and curl-free parts separately, leading to a HHD-like vector field decomposition. Although, they do not consider the harmonic component in their study, it appears that the harmonic component can be computed as the residual. Fig. 8 shows their results, in which they use a Gaussian scalar RBF $\phi(x) = e^{(-\|x\|^2/2\sigma^2)}$, and obtain

$$K_{df}(x, x') = G_{x,x'}\left[A_{x,x'} + \left((d-1) - \frac{\|x - x'\|^2}{\sigma^2}\right)I\right]$$
$$K_{cf}(x, x') = G_{x,x'}\left[I - A_{x,x'}\right],$$

where

$$G_{x,x'} = \frac{1}{\sigma^2}e^{-\frac{\|x-x'\|^2}{2\sigma^2}}$$
$$A_{x,x'} = \left(\frac{x - x'}{\sigma}\right)\left(\frac{x - x'}{\sigma}\right)^T.$$

One can note a similarity between the method of "learning" vector fields and the Galerkin formulation because the kernels K_{df} and K_{cf} span some divergence-free and curl-free subspaces.

6.6 A Non-HHD Decomposition of Flow Fields

Wiebel et al. [102] propose another two-component vector field decomposition, which is substantially different from the HHD. However, since it is based on a similar goal—decomposing the vector field into components with
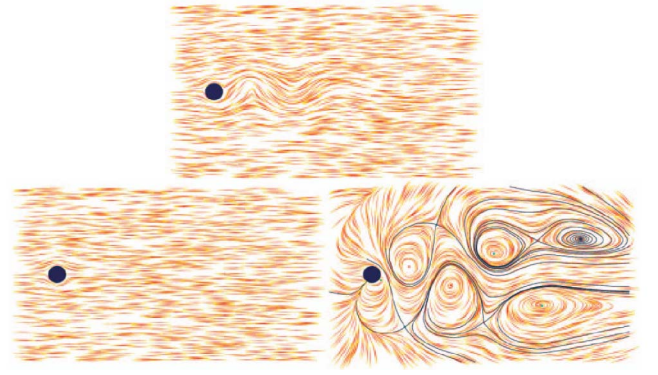

Fig. 9. Results provided by Wiebel et al. [102], showing the cylinder data set (top) decomposed into (bottom) potential and localized flows.

desired properties, it has been included in this survey. Fig. 9 shows their results.

The first component, called the *potential flow* matches the original field on the boundary of a subdomain, but is otherwise simple in the sense that it has vanishing divergence and curl. It represents the laminar flow induced by the geometry of the domain, and its boundary values. In the context of HHD, the potential flow can be seen similar to the harmonic flow $\vec{h}$ in a certain way, because both these flows maintain the property of being both divergence free and curl free. However, it is interesting to see that while the potential flow matches the flow on the boundary of the domain, no such condition is imposed on the harmonic component in HHD. In fact, in the aforementioned computation techniques, the harmonic component is calculated as the residual after calculating the incompressible and irrotational components.

The other (residual) component, called the *localized flow* (or the region-specific flow), promises to capture the entire divergence and curl of the original flow, and hence, provides deeper insights about the features in the original flow. Any analysis that make use of the these two quantities is not affected by the decomposition of the flow. All the critical points (except all saddles) show up in this component. This method works for an arbitrary subregion, with a piecewise smooth boundary. A HHD of the localized flow should further decompose it into incompressible and irrotational components.

7 DISCUSSION

As demonstrated in Fig. 1 and Section 4, the HHD is useful in a large number of applications across a broad spectrum of research communities. Going forward, there is a need for a better consistency between the various communities on the topic. This survey attempts to bring together the diverging branches of research in different communities on this common topic of interest. It presents a comprehensive discussion on the theory and practice of the HHD and intends to provide a solid starting point for future research. While the topic is too extensive and spans too many communities to be fully captured in a single article, the goal is to include a representative cross section of the relevant literature across research areas. Furthermore, this paper includes a notationally consistent discussion on the theory of the HHD to provide an entry point to the area as well as a chronological survey to convey the historical development

of the area. Finally, a detailed discussion on the different boundary conditions is provided aimed at clarifying and unifying some of the recent results.

Nevertheless, some open questions related to the HHD remain to be explored, both theoretical and practical. For instance, the effect of boundary conditions on the topology of the resulting components needs to be studied more thoroughly. Theoretical results of the Hodge decomposition using exterior calculus have already been successfully borrowed and applied to analysis, visualization, and design of vector fields. However, a better understanding of their numerical performance is needed, with respect to its convergence and L^2-orthogonality, especially in the graphics and visualization community.

On a more applied front, one may expect to see a step up in the dimensionality of some recent computation techniques. For example, a SPH technique for 3D vector fields and a LS-FEM like technique for PL vector fields may prove really useful. Moreover, there is a need for further exploration of different boundary conditions aiming for topological consistency between the original field and the resulting components.

ACKNOWLEDGMENTS

REFERENCES

[1] R. Abraham, J.E. Marsden, and T. Ratiu, *Manifolds, Tensor Analysis and Applications,* vol. 75, Applied Math. Science, second ed. Springer-Verlag, 1988.

[2] E. Ahusborde, M. Azaiez, and J.-P. Caltagirone, "A Primal Formulation for the Helmholtz Decomposition," *J. Computational Physics,* vol. 225, no. 1, pp. 13-19, 2007.

[3] K. Aki and P.G. Richards, *Quantitative Seismology.* Univ. Science Books, 2002.

[4] M. Akram and V. Michel, "Regularisation of the Helmholtz Decomposition and its Application to Geomagnetic Field Modelling," *Int'l J. Geomath.,* vol. 1, no. 1, pp. 101-120, 2010.

[5] C. Amrouche, C. Bernardi, M. Dauge, and V. Girault, "Vector Potentials in Three-Dimensional Nonsmooth Domains," *Math. Methods in the Applied Sciences,* vol. 21, pp. 823-864, 1998.

[6] H. Aref, N. Rott, and H. Thomann, "Gröbli's Solution of the Three-Vortex Problem," *Ann. Rev. Fluid Mechanics,* vol. 24, pp. 1-21, 1992.

[7] G. Arfken, *Mathematical Methods for Physicists,* second ed. Academic Press, 1970.

[8] G. Auchmuty, "Potential Representation of Incompressible Vector Fields," *Nonlinear Problems in Applied Mathematics,* pp. 43-49, SIAM, 1995.

[9] J.B. Bell, P. Colella, and H.M. Glaz, "A Second Order Projection Method for the Incompressible Navier-Stokes Equations," *J. Computational Physics,* vol. 85, pp. 257-283, 1989.

[10] J.B. Bell and D.L. Marcus, "A Second-Order Projection Method for Variable-Density Flows," *J. Computational Physics,* vol. 101, pp. 334-348, 1992.

[11] H. Bhatia, G. Norgard, V. Pascucci, and P.-T. Bremer, "Comments on the 'Meshless Helmholtz-Hodge Decomposition'," *IEEE Trans. Visualization and Computer Graphics,* vol. 19, no. 3, pp. 527-528, Mar. 2013.

[12] O. Blumenthal, "Über Die Zerlegung Unendlicher Vektorfelder," *Mathematische Annalen,* vol. 61, no. 2, 235-250, 1905.

[13] H. Braun and A. Hauck, "Tomographic Reconstruction of Vector Fields," *IEEE Trans. Signal Processing,* vol. 39, no. 2, pp. 464-471, Feb. 1991.

[14] R. Bridson, *Fluid Simulation For Computer Graphics.* A.K. Peters, 2008.

[15] D.L. Brown, R. Cortez, and M.L. Minion, "Accurate Projection Methods for the Incompressible Navier-Stokes Equations," *J. Computational Physics,* vol. 168, pp. 464-499, 2001.

[16] E.B. Bykhovskiy and N.V. Smirnov, *On Orthogonal Expansions of the Space of Vector Functions Which Are Square-Summable over a Given Domain and the Vector Analysis Operators.* Academy of Sciences USSR Press, 1960.

[17] J. Caltagirone and J. Breil, "A Vector Projection Method for Solving the Navier-Stokes Equations," *Comptes Rendus de l'Académie des Sciences - Series IIB - Mechanics-Physics-Astronomy,* vol. 327, no. 11, pp. 1179-1184, 1999.

[18] J. Cantarella, D. DeTurck, and H. Gluck, "Vector Calculus and the Topology of Domains in 3-Space," *Am. Math. Monthly,* vol. 109, no. 5, pp. 409-442, 2002.

[19] A.J. Chorin, "A Numerical Method for Solving Incompressible Viscous Flow Problems," *J. Computational Physics,* vol. 2, pp. 12-26, 1967.

[20] A.J. Chorin, "Numerical Solution of the Navier-Stokes Equations," *Math. Computations,* vol. 22, pp. 745-762, 1968.

[21] A.J. Chorin, "On the Convergence of Discrete Approximations to the Navier-Stokes equations," *Math. Computations,* vol. 23, pp. 341-353, 1969.

[22] A.J. Chorin and J.E. Marsden, *A Mathematical Introduction to Fluid Mechanics.* Springer, 1993.

[23] F. Colin, R. Egli, and F. Lin, "Computing a Null Divergence Velocity Field Using Smoothed Particle Hydrodynamics," *J. Computational Physics,* vol. 217, no. 2, pp. 680-692, 2006.

[24] R. Courant and D. Hilbert, *Methods of Mathematical Physics.* New York Univ., 1953.

[25] R. Courant, E. Isaacson, and M. Rees, "On the Solution of Nonlinear Hyperbolic Differential Equations by Finite Differences," *Comm. Pure and Applied Math.,* vol. 5, pp. 243-255, 1952.

[26] S.J. Cummins and M. Rudman, "An SPH Projection Method," *J. Computational Physics,* vol. 152, pp. 584-607, 1999.

[27] F.M. Denaro, "On the Application of the Helmholtz-Hodge Decomposition in Projection Methods for Incompressible Flows with General Boundary Conditions," *Int'l J. Numerical Methods in Fluids,* vol. 43, pp. 43-69, 2003.

[28] E. Deriaz and V. Perrier, "Divergence-Free and Curl-Free Wavelets in 2D and 3D, Application to Turbuent Flows," *J. Turbulence,* vol. 7, no. 3, pp. 1-37, 2006.

[29] E. Deriaz and V. Perrier, "Direct Numerical Simulation of Turbulence Using Divergence-Free Wavelets," *Multiscale Modeling and Simulation,* vol. 7, no. 3, pp. 1101-1129, 2008.

[30] E. Deriaz and V. Perrier, "Orthogonal Helmholtz Decomposition in Arbitrary Dimension using Divergence-Free and Curl-Free Wavelets," *Applied and Computational Harmonic Analysis,* vol. 26, no. 2, pp. 249-269, 2009.

[31] W. Weinan and J.G. Liu, "Projection Method I: Convergence and Numerical Boundary Layers," *SIAM J. Numerical Analysis,* vol. 32, no. 4, pp. 1017-1057, 1995.

[32] R. Fedkiw, J. Stam, and H.W. Jensen, "Visual Simulation of Smoke," *Proc. 28th Ann. Conf. Computer Graphics and Interactive Techniques (SIGGRAPH '01),* pp. 15-22, 2001.

[33] M. Fisher, P. Schröder, M. Desburn, and H. Hoppe, "Design of Tangent Vector Fields," *ACM Trans. Graphics,* vol. 26, no. 3, article 56, 2007.

[34] N. Foster and D. Metaxas, "Realistic Animation of Liquids," *Graphical Models and Image Processing,* vol. 58, no. 5, pp. 471-483, 1996.

[35] N. Foster and D. Metaxas, "Modeling the Motion of a Hot, Turbulent Gas," *Proc. 24th Ann. Conf. Computer Graphics and Interactive Techniques (SIGGRAPH '97),* pp. 181-188, 1997.

[36] D. Fujiwara and H. Morimoto, "An L_r Theorem of the Helmholtz Decomposition of Vector Fields," *J. Faculty of Science,* vol. 44, pp. 685-700, 1977.

[37] E.J. Fuselier, "Refined Error Estimates for Matrix-Valued Radial Basis Functions," PhD thesis, Texas A & M Univ., 2006.

[38] H. Gao, M. Mandal, G. Guo, and J. Wan, "Singular Point Detection using Discrete Hodge Helmholtz Decomposition in Fingerprint Images," *Proc. IEEE Int'l Conf. Acoustics Speech and Signal Processing (ICASSP),* pp. 1094-1097, 2010.

[39] J. Geng and Z. Shen, "The Neumann Problem and Helmholtz Decomposition in Convex Domains," *J. Functional Analysis,* vol. 259, pp. 2147-2164, 2010.

[40] D. Georgobiani, N. Mansour, A. Kosovichev, R. Stein, and Å. Nordlund, "Velocity Field Decomposition in 3D Numerical Simulations of Solar Turbulent Convection," *NASA Center for Turbulence Research - Ann. Research Briefs,* pp. 355-340, 2004.

[41] D.J. Griffiths, *Introduction to Electrodynamics,* second ed. Addison Wesley, 1999.

[42] Q. Guo, "Cardiac Video Analysis using the Hodge Helmholtz Field Decomposition," master's thesis, Dept. of Electrical and Computer Eng., Univ. of Alberta, 2004.

[43] Q. Guo, M.K. Mandal, and M.Y. Li, "Efficient Hodge-Helmholtz Decomposition of Motion Fields," *Pattern Recognition Letters,* vol. 26, no. 4, pp. 493-501, 2005.

[44] Q. Guo, M.K. Mandal, G. Liu, and K.M. Kavanagh, "Cardiac Video Analysis Using Hodge-Helmholtz Field Decomposition," *Computers in Biology and Medicine,* vol. 36, no. 1, pp. 1-20, 2006.

[45] R. Guy and A. Fogelson, "Stability of Approximate Projection Methods on Cell-Centered Grids," *J. Computational Physics,* vol. 203, pp. 517-538, 2005.

[46] F.H. Harlow and J.E. Welch, "Numerical Calculation of Time-Dependent Viscous Incompressible Flow of Fluid with Free Surface," *Physics of Fluids,* vol. 8, no. 12, pp. 2182-2189, 1965.

[47] R. Hatton and H. Choset, "Optimizing Coordinate Choice for Locomoting Systems," *Proc. IEEE Int'l conf. Robotics and Automation (ICRA),* pp. 4493-4498, 2010.

[48] W. Hauser, "On the Fundamental Equations of Electromagnetism," *Am. J. Physics,* vol. 38, no. 1, pp. 80-85, 1970.

[49] W. Hauser, *Introduction to the Principles of Electromagnetism.* Addison-Wesley Educational Publishers Inc, 1971.

[50] H. Helmholtz, "Über Integrale der Hydrodynamischen Gleichungen, Welche den Wirbelbewegungen Entsprechen," *J. für die reine und angewandte Mathematik,* vol. 1858, no. 55, pp. 25-55, Jan. 1858.

[51] H. Helmholtz, "On Integrals of the Hydrodynamical Equations, which Express Vortex-Motion," *Philosophical Magazine and J. Science,* vol. 33, no. 226, pp. 485-512, 1867.

[52] J. Hinkle, P.T. Fletcher, B. Wang, B. Salter, and S. Joshi, "4D MAP Image Reconstruction Incorporating Organ Motion," *Proc. 21st Int'l Conf. Information Processing in Medical Imaging, (IPMI),* 2009.

[53] W. Hodge, *The Theory and Applications of Harmonic Integrals.* Cambridge Univ. Press, 1952.

[54] M.S. Ingber and S.N. Kempka, "A Galerkin Implementation of the Generalized Helmholtz Decomposition for Vorticity Formulations," *J. Computational Physics,* vol. 169, no. 1, pp. 215-237, 2001.

[55] T. Jie and Y. Xubo, "Physically-Based Fluid Animation: A Survey," *Science in China Series F: Information Sciences,* vol. 52, no. 1, pp. 1-17, 2007.

[56] S.A. Johnson, J.F. Greenleaf, M. Tanaka, and G. Flandro, *Acoustical Holography,* vol. 7. Plenum Press, 1977.

[57] D.D. Joseph, "Helmholtz Decomposition Coupling Rotational to Irrotational Flow of a Viscous Fluid," *Proc. Nat'l Academy of Sciences of USA,* vol. 103, no. 39, pp. 14272-14277, 2006.

[58] J. Kim and P. Moin, "Application of a Fractional-Step Method to Incompressible Navier-Stokes Equations," *J. Computational Physics,* vol. 59, no. 2, pp. 308-323, 1985.

[59] D.H. Kobe, "Helmholtz Theorem for Antisymmetric Second-Rank Tensor Fields and Electromagnetism with Magnetic Monopoles," *Am. J. Physics,* vol. 52, no. 4, pp. 354-358, 1984.

[60] D.H. Kobe, "Helmholtz's Theorem Revisited," *Am. J. Physics,* vol. 54, no. 6, pp. 552-554, 1986.

[61] K. Kodaira, "Harmonic Fields in Riemannian Manifolds," *Annals of Math.,* vol. 50, pp. 587-665, 1949.

[62] O.A. Ladyzhenskaja, *The Mathematical Theory of Viscous Incompressible Flow.* Gordon and Breach, 1963.

[63] H. Lamb, *Hydrodynamics,* sixth ed. Cambridge Univ. Press, 1932.

[64] F. Losasso, F. Gibou, and R. Fedkiw, "Simulating Water and Smoke with an Octree Data Structure," *ACM Trans. Graphics,* vol. 23, pp. 457-462, 2004.

[65] L.B. Lucy, "A Numerical Approach to the Testing of the Fission Hypothesis," *The Astronomical J.,* vol. 82, pp. 1013-1024, 1977.

[66] I. Macêdo and R. Castro, "Learning Divergence-Free and Curl-Free Vector Fields with Matrix-Valued Kernels," technical report, Instituto de Matemática Pura e Aplicada, Rio de Janeiro, Brazil, 2010.

[67] N.N. Mansour, A. Kosovichev, D. Georgobiani, A. Wray, and M. Miesch, "Turbulence Convection and Oscillations in the Sun," *Proc. SOHO14/GONG Workshop, "Helio- and Astero-Seismology: Towards a Golden Future,"* 2004.

[68] S.F. McCormick, "The Finite Volume Method," *Multilevel Adaptive Methods for Partial Differential Equations,* chapter 3, vol. 6. SIAM, 1989.

[69] C.A. Micchelli and M. Pontil, "On Learning Vector-Valued Functions," *Neural Computation,* vol. 17, pp. 177-204, 2005.

[70] B.P. Miller, "Interpretations from Helmholtz Theorem in Classical Electromagnetism," *Am. J. Physics,* vol. 52, p. 948, 1984.

[71] C. Min and F. Gibou, "A Second Order Accurate Projection Method for the Incompressible Navier-Stokes Equations on Non-Graded Adaptive Grids," *J. Computational Physics,* vol. 219, pp. 912-929, 2006.

[72] C. Min, F. Gibou, and H.D. Ceniceros, "A Supra-Convergent Finite Difference Scheme for the Variable Coefficient Poisson Equation on Non-Graded Grids," *J. Computational Physics,* vol. 218, no. 1, pp. 123-140, 2006.

[73] Y. Mochizuki and A. Imiya, "Spatial Reasoning for Robot Navigation Using the Helmholtz-Hodge Decomposition of Omni-directional Optical Flow," *Proc. 24th Int'l Conf. Image and Vision Computing (IVCNZ),* pp. 1-6, 2009.

[74] J.J. Monaghan, "Smoothed Particle Hydrodynamics," *Ann. Rev. of Astronomy and Astrophysics,* vol. 30, pp. 543-574, 1992.

[75] L. Morino, "Helmholtz Decomposition Revisited: Vorticity Generation and Trailing Edge Condition," *Computational Mechanics,* vol. 1, pp. 65-90, 1986.

[76] F.J. Narcowich and J.D. Ward, "Generalized Hermite Interpolation Via Matrix-Valued Conditionally Positive Definite Functions," *Math. of Computations,* vol. 63, no. 208, pp. 661-687, 1994.

[77] D.Q. Nguyen, R. Fedkiw, and H.W. Jensen, "Physically based Modeling and Animation of Fire," *ACM Trans. Graphics,* vol. 21, pp. 721-728, 2002.

[78] S.J. Norton, "Tomographic Reconstruction of 2-D Vector Fields: Applications to Flow Imaging," *Geophysics J. Int'l,* vol. 97, no. 1, pp. 161-168, 1988.

[79] S.J. Norton, "Unique Tomographic Reconstruction of Vector Fields Using Boundary Data," *IEEE Trans. Image Processing,* vol. 1, no. 3, pp. 406-412, July 1992.

[80] B. Palit, A. Basu, and M. Mandal, "Applications of the Discrete Hodge-Helmholtz Decomposition to Image and Video Processing," *Proc. First Int'l Conf. Pattern Recognition and Machine Intelligence,* S. Pal, S. Bandyopadhyay, and S. Biswas, eds., pp. 497-502, 2005.

[81] F. Petronetto, A. Paiva, M. Lage, G. Tavares, H. Lopes, and T. Lewiner, "Meshless Helmholtz-Hodge Decomposition," *IEEE Trans. Visualization and Computer Graphics,* vol. 16, no. 2, pp. 338-342, Mar./Apr. 2010.

[82] M. Pharr and G. Humphreys, *Physically Based Rendering: From Theory to Implementation.* Morgan Kaufmann Publishers, Inc., 2004.

[83] K. Polthier and E. Preuß, "Variational Approach to Vector Field Decomposition," *Proc. Eurographics Workshop Scientific Visualization,* 2000.

[84] K. Polthier and E. Preuß, "Identifying Vector Fields Singularities Using a Discrete Hodge Decomposition," *Mathematical Visualization III,* H.C. Hege, K. Polthier, eds., pp. 112-134, Springer, 2003.

[85] S. Popinet, "A Tree-Based Adaptive Solver for the Incompressible Euler Equations in Complex Geometries," *J. Computational Physics,* vol. 190, pp. 572-600, 2003.

[86] J.L. Prince, "Convolution Backprojection Formulas for 3-D Vector Tomography with Application to MRI," *IEEE Trans. Image Processing,* vol. 5, no. 10, pp. 1462-1472, Oct. 1996.

[87] R. Scharstein, "Helmholtz Decomposition of Surface Electric Current in Electromagnetic Scattering Problems," *Proc. 23rd Southeastern Symp. System Theory,* pp. 424-426, 1991.

[88] N. Schleifer, "Differential Forms as a Basis for Vector Analysis - with Applications to Electrodynamics," *Am. J. Physics,* vol. 51, no. 45, p. 1983, 1983.

[89] G. Schwarz, *Hodge Decomposition - A Method for Solving Boundary Value Problems.* Springer, 1995.

[90] J.M. Solomon and W.G. Szymczak, "Finite Difference Solutions for the Incompressible Navier-Stokes Equations Using Galerkin Techniques," *Proc. Fifth IMACS Int'l Symp. Computer Methods for Partial Differential Equations,* June 1984.

[91] W. Sprössig, "On Helmholtz Decompositions and their General-izations - An Overview," *Math. Methods in the Applied Sciences,* vol. 33, pp. 374-383, 2010.

[92] J. Stam, "Stable Fluids," *Proc. ACM SIGGRAPH '99,* pp. 121-128, 1999.

[93] J. Stam, "A Simple Fluid Solver Based on the FFT," *J. Graphics Tools,* vol. 6, pp. 43-52, 2002.

[94] J. Stam and E. Fiume, "Depicting Fire and Other Gaseous Phenomena Using Diffusion Processes," *Proc. ACM SIGGRAPH '95,* pp. 129-136, 1995.

[95] R. Stein and Å. Nordlund, "Realistic Solar Convection Simula-tions," *Solar Physics,* vol. 192, pp. 91-108, 2000.

[96] A.B. Stephens, J.B. Bell, J.M. Solomon, and L.B. Hackerman, "A Finite Difference Galerkin Formulation for the Incompressible Navier-Stokes Equations," *J. Computational Physics,* vol. 53, pp. 152-172, 1984.

[97] Y. Tong, S. Lombeyda, A. Hirani, and M. Desbrun, "Discrete Multiscale Vector Field Decomposition," *ACM Trans. Graphics,* vol. 22, no. 3, pp. 445-452, 2003.

[98] J. van Kan, "A Second-Order Accurate Pressure-Correction Scheme for Viscous Incompressible Flow," *SIAM J. Scientific and Statistical Computing,* vol. 7, no. 3, pp. 870-891, 1986.

[99] K. Wang Weiwei, Y. Tong, M. Desburn, and P. Schröder, "Edge Subdivision Schemes and the Construction of Smooth Vector Fields," *ACM Trans. Graphics,* vol. 25, no. 3, pp. 1041-1048, 2006.

[100] H. Weyl, "The Method of Orthogonal Projection in Potential Theory," *Duke Math. J.,* vol. 7, no. 7, pp. 411-444, 1940.

[101] A. Wiebel, "Feature Detection in Vector Fields Using the Helmholtz-Hodge Decomposition," Diploma thesis, Diplomar-beit, Univ. Kaiserslautern, 2004.

[102] A. Wiebel, C. Garth, and G. Scheuermann, "Computation of Localized Flow for Steady and Unsteady Vector Fields and its Applications," *IEEE Trans. Visualization and Computer Graphics,* vol. 13, no. 4, pp. 641-651, July/Aug. 2007.
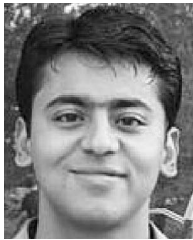
Harsh Bhatia received the BTech degree in information and communication technology from DA-IICT, India in 2007, and is currently a graduate student in computer science at the Scientific Computing and Imaging (SCI) Institute at the University of Utah, and a scholar at the Lawrence Livermore National Laboratory (LLNL). His research interests include topologi-cal analysis of scalar and vector fields, uncer-tainty visualization, graphics and scientific visualization, and modeling and simulation. He is a student member of the IEEE.
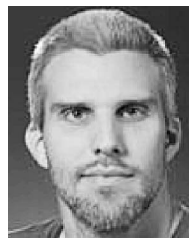
Gregory Norgard received the BS degree in mathematics from the University of Nebraska-Lincoln in 2003, and the PhD degree in applied mathematics from the University of Colorado Boulder in 2009. He is a research scientist at the Numerica Corporation located in Fort Collins, Colorado. Before joining Numerica, he was a postdoctoral researcher at Lawrence Livermore National Laboratory (LLNL). His research inter-ests include data fusion, uncertainty manage-ment, computational topology, and computational fluid dynamics.

Valerio Pascucci received the EE laurea (master's) degree from the University La Sa-pienza in Rome, Italy, in December 1993, as a member of the Geometric Computing Group, and the PhD degree in computer science from Purdue University in May 2000. He is a faculty member at the Scientific Computing and Ima-ging (SCI) Institute at the University of Utah. Before joining SCI, he served as a project leader at the Lawrence Livermore National Laboratory (LLNL), Center for Applied Scientific Computing (from May 2000) and as an adjunct professor at the Computer Science Department of the University of California, Davis (from July 2005). Prior to his tenure at CASC, he was a senior research associate at the University of Texas at Austin, Center for Computational Visualization, CS, and TICAM Departments. He is a member of the IEEE.

Peer-Timo Bremer received the diploma in mathematics and computer science from the Leipniz University in Hannover, Germany, in 2000, and the PhD degree in computer science from the University of California, Davis, in 2004. He is a computer scientist and project leader at the Center for Applied Scientific Computing at the Lawrence Livermore National Laboratory (LLNL) and an associated director for Research at the Center for Extreme Data Managment, Analysis, and Visualization at the University of Utah. Prior to his tenure at CASC, he was a postdoctoral research associate at the University of Illinois, Urbana-Champaign. He is a member of the IEEE Computer Society and the IEEE.

▷ **For more information on this or any other computing topic, please visit our Digital Library at** www.computer.org/publications/dlib.